RPE65 variant p.(E519K) causes a novel dominant adult-onset maculopathy in 83 affected individuals

Eline Van Vooren

  Department of Biomolecular Medicine, Ghent University, Ghent, Belgium   https://orcid.org/0000-0002-8731-1199

Filip Van den Broeck

  Department of Head and Skin, Ghent University, Ghent, Belgium; Department of Ophthalmology, Ghent University Hospital, Ghent, Belgium   https://orcid.org/0009-0006-3330-6497

Quinten Mahieu

  Department of Biomolecular Medicine, Ghent University, Ghent, Belgium   https://orcid.org/0000-0002-0850-1745

Eline Geens

  Department of Biomolecular Medicine, Ghent University, Ghent, Belgium

Mattias Van Heetvelde

  Department of Biomolecular Medicine, Ghent University, Ghent, Belgium

Marieke De Bruyne

  Center for Medical Genetics, Ghent University Hospital, Ghent, Belgium   https://orcid.org/0000-0001-6636-5537

Stijn Van de Sompele

  Center for Medical Genetics, Ghent University Hospital, Ghent, Belgium   https://orcid.org/0000-0002-3294-0668

Sheetal Uppal

  Laboratory of Retinal Cell and Molecular Biology, National Eye Institute, NIH, Bethesda, United States
https://orcid.org/0000-0002-3685-8602

Eugenia Poliakov

  Laboratory of Retinal Cell and Molecular Biology, National Eye Institute, NIH, Bethesda, United States

Claire-Marie Dhaenens

  Univ. Lille, Inserm, CHU Lille, U1172-LilNCog-Lille Neuroscience & Cognition, F-59000 Lille, France
https://orcid.org/0000-0003-4719-4124

Cheryl Y. Gregory-Evans

  University of British Columbia, Department of Ophthalmology & Visual Sciences, Vancouver, BC, Canada
https://orcid.org/0000-0001-8613-0460

Lies Hoefsloot

  Department of Clinical Genetics, Erasmus Medical Centre, Rotterdam, The Netherlands
https://orcid.org/0009-0000-3444-9955

Adriana Iglesias Gonzalez

Department of Clinical Genetics, Erasmus Medical Centre, Rotterdam, The Netherlands

https://orcid.org/0000-0001-5532-764X

Susanne Kohl

Institute for Ophthalmic Research, Centre for Ophthalmology, University Hospital Tübingen, Germany

https://orcid.org/0000-0002-6438-6331

Theresia Zuleger

Institute of Medical Genetics and Applied Genomics, University Hospital Tübingen, Germany

Tanguy Demaret

Centre de Génétique Humaine, Institut de Pathologie et de Génétique, Gosselies, Belgium

https://orcid.org/0000-0001-7605-9031

Dominant RPE65-E519K Consortium

Sari Tuupanen

Blueprint Genetics, Espoo, Finland

Joke Ruys

Department of Ophthalmology, Ghent University Hospital, Ghent, Belgium; Department of Ophthalmology, Vitaz, Sint-Niklaas, Belgium

Luc Van Os

Department of Ophthalmology, Antwerp University Hospital, Antwerp, Belgium   https://orcid.org/0000-0001-7879-4232

Elise Platteau

Department Ophthalmology, Maria Middelares Hospital, Ghent, Belgium

Julie Jacob

Department of Ophthalmology, UZ Leuven, Leuven, Belgium   https://orcid.org/0000-0002-4716-6820

Sascha Vermeer

Center for Human Genetics, UZ Leuven, Leuven, Belgium   https://orcid.org/0000-0001-7625-1912

Laurence Postelmans

Department of Ophthalmology, CHU Brugmann, Brussels, Belgium

Karin Dahan

Centre de Génétique Humaine, Institut de Pathologie et de Génétique, Gosselies, Belgium

Isabelle Maystadt

Centre de Génétique Humaine, Institut de Pathologie et de Génétique, Gosselies, Belgium

https://orcid.org/0000-0001-7170-8186

Florence Rasquin

Department of ophthalmology, Erasme Hospital, Université Libre de Bruxelles, Brussels, Belgium

Alberta A.H.J. Thiadens

Department of Ophthalmology, Erasmus Medical Centre, Rotterdam, The Netherlands

https://orcid.org/0000-0002-4911-9462

Kirk A.J. Stephenson

University of British Columbia, Department of Ophthalmology & Visual Sciences, Vancouver, BC, Canada

Narin Sheri

Department of Ophthalmology and Visual Sciences, University of Alberta, Edmonton, Canada

Vasily Smirnov

Univ. Lille, Inserm, CHU Lille, U1172-LilNCog-Lille Neuroscience & Cognition, F-59000 Lille, France; Sorbonne Université, INSERM, CNRS, Institut de la Vision, Paris, France   https://orcid.org/0000-0003-4172-514X

Ian M. MacDonald

Department of Ophthalmology and Visual Sciences, University of Alberta, Edmonton, Canada https://orcid.org/0000-0001-7472-8385

Kevin Gregory-Evans

University of British Columbia, Department of Ophthalmology & Visual Sciences, Vancouver, BC, Canada https://orcid.org/0000-0003-3572-3105

T. Michael Redmond

Laboratory of Retinal Cell and Molecular Biology, National Eye Institute, NIH, Bethesda, United States https://orcid.org/0000-0002-1813-5291

Julie De Zaeytijd

Department of Ophthalmology, Ghent University Hospital, Ghent, Belgium   https://orcid.org/0000-0003-4035-6389

Bart P. Leroy

Center for Medical Genetics, Ghent University Hospital, Ghent, Belgium; Department of Head and Skin, Ghent University, Ghent, Belgium; Department of Ophthalmology, Ghent University Hospital, Ghent, Belgium; Division of Ophthalmology and Center for Cellular and Molecular Therapeutics, Children's Hospital of Philadelphia, Philadelphia, PA, United States   https://orcid.org/0000-0002-9899-2081

Miriam Bauwens

`miriam.bauwens@ugent.be`

Department of Biomolecular Medicine, Ghent University, Ghent, Belgium   https://orcid.org/0000-0003-0402-9006

Elfride De Baere

`elfride.debaere@ugent.be`

Department of Biomolecular Medicine, Ghent University, Ghent, Belgium   https://orcid.org/0000-0002-5609-6895

Research Article

Additional Declarations: The authors declare no competing interests.

RPE65 variant p.(E519K) causes a novel dominant adult-onset maculopathy in 83 affected individuals

Eline Van Vooren[1,2]*, Filip Van den Broeck[3,4]*, Quinten Mahieu[1,2], Eline Geens[1,2], Mattias Van Heetvelde[1,2], Marieke De Bruyne[2], Stijn Van de Sompele[2], Sheetal Uppal[5], Eugenia Poliakov[5], Claire-Marie Dhaenens[6], Cheryl Y. Gregory-Evans[7], Lies Hoefsloot[8], Adriana Iglesias Gonzalez[8], Susanne Kohl[9], Theresia Zuleger[10], Tanguy Demaret[11], Dominant RPE65-p.(E519K) Consortium, Sari Tuupanen[12], Joke Ruys[4,13], Luc Van Os[14], Elise Platteau[15], Julie Jacob[16], Sascha Vermeer[17], Laurence Postelmans[18], Karin Dahan[11], Isabelle Maystadt[11], Florence Rasquin[19], Alberta A.H.J. Thiadens[20], Kirk A.J. Stephenson[7], Narin Sheri[21], Vasily Smirnov[6,22], Ian M. MacDonald[21], Kevin Gregory-Evans[7], T. Michael Redmond[5], Julie De Zaeytijd[4°], Bart P. Leroy[2,3,4,23°], Miriam Bauwens[1,2°], Elfride De Baere[1,2°]

[1]Department of Biomolecular Medicine, Ghent University, Ghent, Belgium
[2]Center for Medical Genetics, Ghent University Hospital, Ghent, 9000, Belgium
[3]Department of Head and Skin, Ghent University, Ghent, 9000, Belgium
[4]Department of Ophthalmology, Ghent University Hospital, Ghent, 9000, Belgium
[5]Laboratory of Retinal Cell and Molecular Biology, National Eye Institute, NIH, Bethesda, 20892, United States
[6]Univ. Lille, Inserm, CHU Lille, U1172-LilNCog-Lille Neuroscience & Cognition, F-59000 Lille, 59000, France
[7]University of British Columbia, Department of Ophthalmology & Visual Sciences, Vancouver, BC, V6T 1Z4, Canada
[8]Department of Clinical Genetics, Erasmus Medical Centre, Rotterdam, 3015, The Netherlands
[9]Institute for Ophthalmic Research, Centre for Ophthalmology, University Hospital Tübingen, 72074, Germany;
[10]Institute of Medical Genetics and Applied Genomics, University Hospital Tübingen, 72074, Germany
[11]Centre de Génétique Humaine, Institut de Pathologie et de Génétique, Gosselies, 6041, Belgium
[12]Blueprint Genetics, Espoo, 02150, Finland
[13]Department of Ophthalmology, Vitaz, Sint-Niklaas, 9100, Belgium
[14]Department of Ophthalmology, Antwerp University Hospital, Antwerp, 2650, Belgium
[15]Department Ophthalmology, Maria Middelares Hospital, Ghent, 9000, Belgium
[16]Department of Ophthalmology, UZ Leuven, Leuven, 3000, Belgium
[17] Center for Human Genetics, UZ Leuven, Leuven, 3000, Belgium
[18]Department of Ophthalmology, CHU Brugmann, Brussels, 1020, Belgium
[19]Department of ophthalmology, Erasme Hospital, Université Libre de Bruxelles, Brussels, 1070, Belgium
[20]Department of Ophthalmology, Erasmus Medical Center, Rotterdam, 3015, The Netherlands
[21]Department of Ophthalmology and Visual Sciences, University of Alberta, Edmonton, T6G 2R3, Canada
[22]Sorbonne Université, INSERM, CNRS, Institut de la Vision, Paris, 75012, France
[23]Division of Ophthalmology and Center for Cellular and Molecular Therapeutics, Children's Hospital of Philadelphia, Philadelphia, PA, 19104, United States

*Equal contribution as first authors
° Equal contribution as last authors

Correspondence to Elfride De Baere, elfride.debaere@ugent.be and Miriam Bauwens, miriam.bauwens@ugent.be

Abstract

Recessive RPE65-related retinopathy is an inherited retinal disease (IRD) that is a well-established target for gene therapy. Dominant RPE65-related retinopathy, however, due to Irish founder variant p.(D477G), is extremely rare. Here, we report the discovery, replication and characterization of a novel dominant retinopathy caused by RPE65 variant p.(E519K), identified in 83 individuals of European ancestry across IRD registries (Belgian discovery cohort, n=2,873; replication cohort, n=18,796). Long-read sequencing-based haplotyping revealed a shared region of 464 kb, supporting a founder effect. Genotype-phenotype data support dominant inheritance and phenotypic variability respectively, characterized by late-onset macular dystrophy with two main subtypes, a pathognomonic mottled subtype and a pattern dystrophy subtype. Functional studies showed that the p.(E519K) variant affects RPE65 enzymatic activity, correlating with lower protein expression. Protein modelling and cellular thermal shift assays further supported a destabilizing effect on protein structure. Overall, our work provides strong genetic, clinical, molecular and functional evidence for a novel dominant RPE65 retinopathy in multiple families in Europe and North America due to a Belgian founder variant. This discovery reduces the diagnostic gap in dominant IRD, particularly in individuals of European ancestry. Finally, it lays the foundation for developing therapeutic strategies targeting dominant RPE65 retinopathy.

Introduction

Approximately two million people worldwide are affected by inherited retinal diseases (IRD), a clinically and genetically heterogeneous group of disorders leading to progressive or stable vision loss[1,2]. Over 290 genes have been implicated in IRD, one of which is *RPE65* (retinal pigment epithelium-specific 65 kDa), encoding a key enzyme in the visual cycle, which catalyzes the isomerization of all-*trans* retinyl ester to 11-*cis* retinol[3–5]. Biallelic pathogenic variants in the *RPE65* gene (OMIM*180069) are implicated in different forms of autosomal recessive (AR) IRD, including Leber congenital amaurosis type 2, early-onset severe retinal dystrophy, and retinitis pigmentosa. Patients with AR *RPE65*-IRD manifest a generalized phenotype with congenital or early-onset night blindness, progressive loss of visual field and loss of central vision[6].

Voretigene neparvovec-rzyl (Luxturna®), the first gene therapy for IRD approved by FDA and EMA in 2017 and 2018 respectively, is a gene augmentation therapy involving subretinal injection of adeno-associated virus type 2 vectors containing wild type (WT) *RPE65* complementary DNA (cDNA), resulting in improved light sensitivity, visual field and navigational abilities[7–10]. Eligibility depends on the presence of biallelic (likely) pathogenic *RPE65* variants and sufficient viable outer retinal cells, emphasizing the importance of an early molecular diagnosis.

Autosomal dominant (AD) *RPE65*-IRD has been described only once and is due to the Irish founder variant c.1430A>G, p.(Asp477Gly), also known as p.(D477G). Non-penetrance and large phenotypic variability, ranging from foveal vitelliform lesions to extensive chorioretinal atrophy mimicking choroideremia, have been described in a few families worldwide[11–14]. In p.(D477G)-IRD knock-in mouse models only minimal phenotypic manifestations were observed[15–17]. Possible mechanisms of action involve aberrant RNA splicing and a toxic and/or dominant-negative effect through abnormal aggregate formation[15,17].

94   Here, we describe the discovery, replication, clinical, molecular and functional characterization

95   of a novel AD *RPE65*-related retinopathy in multiple families in Europe and North America due

96   to a Belgian founder variant c.1555G>A, p.(Glu519Lys), hereafter referred to as p.(E519K).

97   Our findings reduce the diagnostic gap in dominant IRD, specifically in individuals of European

98   ancestry, and highlight a novel target for therapy.

Methods

Patients

Index patients and (affected) family members were recruited from Belgian ophthalmology clinics and centers for medical genetics. The study was conducted in accordance with the principles of the Declaration of Helsinki and was approved by the Ethics Committee of Ghent University Hospital (B6702021000312). All included patients consented to the study.

Clinical investigations

The in-house p.(E519K) cohort, for which clinical investigations are described, consists of 65 patients, who have been examined at least once at the Department of Ophthalmology at Ghent University Hospital, Ghent, Belgium, the national referral center for ophthalmic genetics. Prior clinical records were revisited for general and ophthalmologic history, and for ophthalmological data recorded at first and follow-up visits. Ophthalmological data included best-corrected visual acuity (BCVA), ISCEV-standard full-field flash electroretinography in 50% of patients and electro-oculography in five cases (Roland Consult, Brandenburg an der Havel, Germany), anterior segment and dilated fundus examination supplemented with multimodal fundus imaging including spectral-domain optical coherence tomography (OCT), long-wavelength (690 nm) reflectance and short-wavelength (588 nm) autofluorescence (SW-AF) imaging with confocal scanning-laser ophthalmoscopy (Spectralis, Heidelberg Engineering GmbH, Heidelberg, Germany), color fundus photography (Clarus 700, ZEISS, Jena, Germany; and/or TRC-IX50 and TRC-DX50, Topcon Corporation, Tokyo, Japan).

BCVAs were measured using logMAR charts and are expressed in decimal equivalents. Values above 1.00 were limited to 1.00 as testing was not consistently continued beyond this point. Off-chart values were equalized with decimal values as previously described[18]. Five eyes of three patients were excluded for clinical analysis due to comorbidity with a more severe IRD or retinal trauma bringing the total to 125 eyes of 63 cases for clinical analysis. Of these, an additional five eyes (three cases) had their symptomatology and BCVAs excluded due to a

125 comorbidity expected to affect these variables (Table 1). These factors are the reason the total

126 number of cases (denominators) are not the same for every ratio presented.

127 **Short-read whole genome sequencing (srWGS)**

128 Short-read whole genome sequencing (srWGS) was performed for patients F5-III:2, F5-IV:3

129 and F8-II:4. Library preparation and sequencing were performed using the Illumina DNA

130 polymerase chain reaction (PCR)-Free LibraryPrep kit and 150 base pairs (bp) paired-end

131 sequencing (S4, 300 cycles, NovaSeq 6000, Illumina, CA, USA). Data were basecalled using

132 bcl2fastq2 (v2.20)[19] and basecalled reads were subsequently aligned to GRCh38 using BWA-

133 MEM (v0.7.17)[20]. Variant calling for single nucleotide variants (SNVs) was done using

134 HaplotypeCaller from the GATK (v3.3)[21] toolkit and annotation was performed through

135 Ensembl Variant Effect Predictor (v110.0)[22] and dbNSFP (v4)[23]. Post-demultiplexing steps

136 were performed within the bcbio toolkit[24]. Resulting SNV VCF files were analyzed using the in-

137 house tool Seqplorer (https://seqplorer.cmgg.be/user/login/) for coding variants in the RetNet

138 panel (v7, 324 genes) and the online platform Franklin (Genoox, https://franklin.genoox.com/)

139 for coding and non-coding variants in the same panel. Structural variants (SVs) overlapping

140 with this gene panel were assessed using Manta (v1.6.0)[25] and Delly (v0.8.7)[26]. Variants were

141 classified using American College of Medical Genetics and Association for Clinical Genomic

142 Science guidelines with adaptations[27]. The strength of some criteria was altered under certain

143 conditions as recommended in literature[27–31].

144 **Whole exome sequencing (WES)**

145 A subset of index patients underwent WES, revealing p.(E519K) (Table 1, Supplementary

146 Table 1). In addition, targeted sequencing of in-house index patients (F12-II:1, F13-II:2, S08,

147 S09, S11, S13, S14, S17, S18 and S21) was supplemented with WES to exclude the presence

148 of additional (likely) pathogenic variants in IRD genes. Library preparation and sequencing

149 were performed using the SureSelectXT Human All Exon V6 or V7 (Agilent, CA, USA), KAPA

150 HyperExome V1 (Roche) kit or Haloplex target enrichment System (Agilent Technologies Inc.,

151 CA, USA) and 150 bp paired-end sequencing (HiSeq 3000 or NovaSeq 6000, Illumina, CA,

152 USA). Basecalling, demultiplexing, alignment, variant calling and annotation was performed

153 as described for srWGS data, using a bed file to restrict the analysis to coding regions.

154 Resulting SNVs were filtered using the in-house WES analysis tool Seqplorer for the

155 customized RetNet panel (v7). Copy number variations in these genes were assessed using

156 ExomeDepth (v1.1.16)[32].

157 An NGS-based assay, containing 351 IRD genes, was performed for patients F16-II:1, F16-

158 II:2, S32 and S33 using the Blueprint Genetics Retinal Dystrophy Panel[33], while patients S29

159 and S30 underwent sequencing of the Inherited Retinal Disorders Panel by Invitae, containing

160 330 genes[34].

161 Patient S34 underwent high-throughput sequencing of a panel of 226 IRD genes. Coding

162 exons and their flanking intronic regions were captured using the HaloPlex target enrichment

163 System (Agilent Technologies Inc., CA, USA). DNA libraries were sequenced on a NovaSeq

164 sequencer (Illumina). Data analysis was done using an in-house developed pipeline compiling

165 the data obtained from SeqNext (JSI Medical System, Ettenheim, Germany) and GATK

166 software. Copy number variants (CNVs) detection was performed by a quantitative analysis

167 based on the amplicons read depth as previously described[35].

168 The DNA of patient S35 was enriched using Agilent SureSelect DNA, SureSelect OneSeq

169 300kb CNV Backbone and Human All Exon V7 capture, followed by paired-end sequencing

170 (Illumina). Data were demultiplexed with bcl2fastq and reads were mapped using BWA-MEM.

171 Variant calling was performed by the GATK HaplotypeCaller, followed by filtering and

172 annotation with Alissa Interpret software and classification with Alamut Visual. CNV detection

173 was done via the BAM multiscale reference method using depth of coverage analysis and

174 dynamical bins in NexusClinical, which was also used to filter and annotate the detected CNVs.

175 **Targeted sequencing and segregation analysis**

176 A subset of index patients (Table 1, Supplementary table 1) that had previously tested negative

177 for mitochondrial retinopathy, or for *ABCA4*, *BEST1* or *PRPH2* targeted testing, underwent

178 targeted sequencing for p.(E519K). Fifty-one family members underwent segregation analysis

7

179 for p.(E519K). PCRs were performed using Kapa2G Robust Master Mix (2x, Kapa Biosystems,

180 MA, USA), followed by Sanger sequencing using the BrilliantDye™ kit (v3.1, NimaGen,

181 Nijmegen, Netherlands) and run on an ABI3730XL DNA analyzer (Applied Biosystems, MA,

182 USA). Primers used for PCR and sequencing are listed in Supplementary Table 2.

183 **Long-read whole genome sequencing (lrWGS)**

184 Long-read whole genome sequencing (lrWGS) was executed for patients F5-III:2, F5-IV:3, F8-

185 II:3; and F8-II:4. Library preparation was performed using the SQK-LSK114 ligation

186 sequencing kit (Oxford Nanopore Technologies (ONT), United Kingdom), followed by

187 sequencing on a PromethION 24 system (ONT), using an individual FLO-PRO114M (ONT)

188 flow cell for each sample, for a maximum of 72 hours (h). Basecalling was done through Guppy

189 (v.6.4.6, ONT) after which reads were filtered on a minimum length of 100 bases and a

190 minimum average read quality score of 10. Reads were trimmed and mapped to GRCh38.p14

191 via minimap2 (v2.24)[36]. SVs were called with SVIM (v1.4.2)[37], Sniffels2 (v2.0.7)[38], and CuteSV

192 (v2.0.2)[39] after which a consensus VCF was generated using Jasmine (v1.1.5)[40]. SNVs were

193 called using Clair3 (v1.0.5)[41] and phased using WhatsHap (v2.0)[42]. Coverage analysis was

194 done for all alignment files using mosdepth (v0.3.3)[43] and quality metrics were assessed

195 through pycoQC (v2.5.2)[44] and NanoPlot (v1.40.0)[45].

196 **Microsatellite analysis**

197 Microsatellite markers (Supplementary Table 3) were PCR amplified with 10x PCR buffer

198 (Invitrogen, MA, USA), 50 mM $MgCl_2$ (Invitrogen), 1 mM dNTPs (New England Biolabs (NEB),

199 MA, USA), DMSO (Sigma-Aldrich, MO, USA), 5 u/µl Taq (Invitrogen), and 10 µM primer. One

200 µl of product was mixed with 0.3 µl ROX-500 size standard (GeneScan, Freiburg im Breisgau,

201 Germany) and 10 µl Hi-Di formamide (Applied Biosystems). PCR fragments were size

202 fractionated on an ABI3730XL capillary sequencer and data were analyzed using GeneMapper

203 software (v5, Applied Biosystems).

204 **Generation of expression vectors and site-directed mutagenesis**

Human *RPE65* and *CRALBP* cDNAs, obtained from gBlocks (IDT, IA, USA), were subcloned

into bicistronic pVitro2 expression vector (InvivoGen, CA, USA). An expression vector

containing *RPE65* cDNA in the pcDNA3.4 backbone was obtained from GenScript (New

Jersey, USA). The p.(D477G) and p.(E519K) variants were introduced in the *RPE65* sequence

in both vectors, and HA- and MYC-tags were introduced into the *RPE65*-pcDNA3.4 vector,

using the Q5 Site-Directed Mutagenesis Kit (NEB). Primers used to amplify the gBlocks,

mutagenesis PCR and PCR to verify the mutagenesis are listed in Supplementary Table 4.

Cell culture and transient transfection

HEK 293-T cells (ATCC, Virginia, USA) were maintained in Dulbecco's Modified Eagle Medium

(DMEM, Gibco, Thermo Fisher, MA, USA) supplemented with 10% fetal bovine serum (FBS,

Greiner Bio-One, Kremsmünster, Austria) and 1% Penicillin-Streptomycin (Gibco) at 37 °C with

5% CO_2. Adult Retinal Pigment Epithelium-19 (ARPE-19, ATCC) cells were maintained in

DMEM-F12 (Gibco), supplemented with 10% FBS, 1% Penicillin-Streptomycin, 1% Non-

essential amino acids (Gibco), 1% Glutamax supplement (Gibco) and 0.1% Amphotericin B

(Gibco). Cells were seeded, $0.75 - 3 \times 10^4$ cells (12-well plate) and 2.2×10^6 cells (10 cm

culture dish) and transfected using Lipofectamine 3000 transfection agent (Invitrogen) or

TransIT-X2 (Mirus Bio, WI, USA) with 1 mg/ml – 1 µg/ml vector, depending on the experiment.

Negative control samples were transfected without vector.

For the *in vitro* isomerase activity assay, pVitro2 expression plasmids containing either WT-

RPE65 or p.(E519K)-RPE65 were prepared by using QIAprep Maxi kits (Qiagen, CA, USA).

Next, 30 µg of pVitro2 plasmid (WT or mutant) were transfected into human Expi293

suspension cells (Thermo Fisher Scientific) using 40 µl of ExpiFectamine transfection reagent

(Thermo Fisher Scientific). The cells were incubated on an orbital shaker at 37 °C and 8% CO_2

for 16-18 h. At 18 h post transfection Expifectamine 293 Enhancer 1 (150 mL/flask) and

Expifectamine 293 Enhancer 2 (1.5 mL per flask) were added. All-*trans* retinol was added 42

h post-initial transfection, at a final concentration of 2.5 µM. Finally, cells were harvested at 6

h after substrate addition (total 48 h transfection to harvest) for downstream retinoid analysis.

Retinoid extraction, saponification, and retinoid analysis

All procedures were performed under red safelights. For analysis of WT and p.(E519K)-RPE65 activity in Expi293 cells, retinoids were extracted and saponified as described[46] from cells harvested by centrifugation from 30 ml volumes of cultured transfected Expi293 cells. Isomeric retinols were analyzed on 5 μm particle LiChrospher Si-60 (Alltech, IL, USA) normal phase columns (2 × 250 mm) on an Agilent 1100/1200 series HPLC system (Agilent Technologies, DE, USA), in hexane mobile phase containing ethyl acetate (11.2%):dioxane (2.0%):octanol (1.4%), following Landers & Olson, 1988[47], as earlier modified[46]. Data were analyzed using ChemStation32 software (Agilent).

Western blot

Proteins were isolated using radioimmunoprecipitation assay buffer (RIPA, 94%, Sigma-Aldrich), protease inhibitor (4%, Roche, Basel, Switzerland), phosphatase inhibitor 2 (1%, Sigma-Aldrich), and phosphatase inhibitor 3 (1%, Sigma-Aldrich). Assessment of protein yields was performed according to the Pierce BCA protein assay protocol (Thermo Fisher). Total protein (15-25 µg) was separated by electrophoresis on Nu-Page 4-12% Bis-Tris Gel (Invitrogen) under reducing conditions and transferred to a nitrocellulose membrane (Invitrogen). Membranes were blocked with 5% membrane blocking agent (Cytiva, MA, USA) and incubated with either anti-RPE65 antibody (1:600, 17939-1-AP, Proteintech Europe, Manchester, UK), anti-CRALBP (1:4000, ab1501, Abcam, Cambridge, UK), or anti-ß-tubulin (1:2500, ab6046, Abcam) 1.5 - 2 h at room temperature. Membranes were washed with 1x Tris-buffered saline with 0.5% Tween20 and incubated with secondary anti-rabbit or mouse antibody (1:2500, Cell Signaling Technology, MA, USA). Membranes were developed with SuperSignal West Dura Extended Duration Substrate (Thermo Fisher). Expression levels of CRALBP were used to evaluate transfection efficiency and to normalize RPE65 expression. Quantification of RPE65 and CRALBP expression was performed using the ImageLab software (v6.1, Bio-Rad, CA, USA).

Cellular thermal shift assay (CETSA)

259   Ten million HEK 293-T cells were transfected (single or co-transfected) with 1 mg/ml WT-

260   RPE65, p.(D477G) and/or p.(E519K) expression vector as described above. Forty-eight h after

261   transfection, the cells were pelleted, dissolved in 1 ml 1x PBS (Gibco) and distributed over 12

262   tubes and spun down. Eighty μl of PBS was removed and each tube was incubated at a

263   specific temperature within the following range 30 – 66.9 °C. Proteins were extracted by

264   repeated freeze-thaw cycles using liquid nitrogen, followed by addition of 80 μl 1x PBS and

265   ultracentrifugation (Optima TLX ultracentrifuge, Beckman Coulter, CA, USA). The supernatant

266   was transferred, and protein concentrations were determined by the Pierce BCA protein assay

267   kit (Thermo Fisher). Western blot was performed using anti-RPE65 antibody as described

268   above.

269   **Minigene assays**

270   To test the effect of *RPE65* variants p.(E519K) and p.(D477G) on splicing *in vitro* splice assays

271   were used. A 3.4 kb genomic segment of *RPE65* spanning exons 11-14 was amplified from

272   human genomic control DNA (Roche). The WT-*RPE65* PCR product was restricted and

273   subsequently subcloned into the pSPL3_2096 vector, a derivative of the exon-trapping vector

274   pSPL3 (Invitrogen-Life Technologies, Carlsbad, CA, USA), containing two HIV-TAT exons

275   (TAT1, TAT2), flanking the insert. Mutant constructs were obtained using the Q5 Site-Directed

276   Mutagenesis kit (NEB, MA, USA). Integrity of constructs was assessed using ONT long-read

277   sequencing (Plasmidsaurus, Eugene, OR, USA). Constructs were transfected in HEK293T

278   cells using Lipofectamine 3000 (Invitrogen). After 24 h, total RNA was extracted (RNeasy Mini

279   Kit, Qiagen Benelux, Antwerp, Belgium) and used as input to obtain cDNA (iScript Select cDNA

280   synthesis kit, Bio-Rad Laboratories). cDNA was PCR amplified with pSPL3 exon primers and

281   separated via agarose gel (2% TBE) electrophoresis, followed by Sanger sequencing (Applied

282   Biosystems), next generation sequencing (NGS, MiSeq, Illumina) and ONT long-read

283   sequencing (Eurofins Genomics, Germany). Primers used for cDNA synthesis and cDNA PCR

284   are listed in Supplementary Table 5.

285 To calculate exon ratios NGS and ONT data was aligned against the corresponding construct

286 sequence using STAR (v2.7)[48] and minimap2 (v2.24)[36] respectively. Coverage for each

287 position of the construct was determined using samtools depth (v1.18)[49], and mean coverage

288 was calculated for exons included in the construct. Cumulative bar graphs for the relative

289 coverage for each region were made with ggplot2 (v3.4.3) in RStudio (v2023.12.1+402).

290 **Co-immunoprecipitation (Co-IP)**

291 Plasmids expressing HA-tagged WT-RPE65 and MYC-tagged p.(D477G) or p.(E519K)-

292 RPE65 were either individually or co-transfected at an equal molar ratio in ARPE-19 cells,

293 using TransIT-X2 (Mirus Bio, WI, USA) at 1 mg/ml and a 3:1 TransIT-X2/DNA ratio. At 48 h

294 post transfection, total cellular proteins were extracted as described above. Co-IP was

295 performed with protein A Dynabeads following manufacturer's protocol (Invitrogen, MA, USA)

296 using the anti-MYC (2 µg, ab9106, Abcam), the anti-HA (2 µg, ab9110, Abcam) and the anti-

297 IGG antibodies (4 µg, ab2410, Abcam). Western blot was performed as mentioned earlier with

298 the abovementioned anti-MYC (1:2000) and anti-HA (1:4000) antibodies.

299 **RPE65 protein crystal structure and modeling with AlphaFold**

300 All monomer protein structures were modeled using the standalone version of AlphaFold

301 (v2.0.0)[50]. WT RPE65 was modeled using a fasta file containing the UniProt sequence

302 (https://www.uniprot.org/uniprotkb/Q16518/entry#sequences) as the only input for the '–

303 fasta_paths' flag. For missense isoforms modeling, this sequence was adapted to the

304 predicted amino acid sequence resulting from each respective missense variant. Dimer

305 structure predictions were modeled using AlphaFold (v2.3.1) with the 'multimer' model preset.

306 Fasta files, used as the only input for the '–fasta_paths' flag, contained only the two respective

307 monomer structure sequences for each dimer structure prediction of interest. The ranked0

308 structures and crystal structures, 3FSN[51] and 4RYX[52] were visualized using UCSF ChimeraX

309 (v1.7.1, RBVI with support of the National Institutes of Health, University of California, CA,

310 USA). ChimeraX was also used to perform an electrostatic surface analysis.

311 *In silico* **predictions**

312   *In silico* (splice) prediction scores were obtained for NM_000329.3: c.1430A>G (chr1:

313   g.68431085T>C) and NM_000329.3: c.1555G>A (chr1:g.68429823C>T) using dbNSFP

314   (v4.7)[53] , PolyPhen-2[54], MutationTaster2021[55], Mutscore[56], AlphaMissense[57], SpliceAI lookup

315   (Max distance 5000)[58] and Aggrescan[59].

316   **Statistical analysis**

317   Data visualization and statistical analyses were performed with GraphPad Prism v10.2.0 for

318   macOS (GraphPad Software, MA, USA). A Kruskal-Wallis test with Dunn's multiple

319   comparisons test was used to compare protein expression of Western blot, while a non-linear

320   regression was used to generate the melting curves for CETSA.

Results

A novel *RPE65*-related dominant retinopathy caused by monoallelic variant p.(E519K)

WGS was performed in three WES-prescreened patients (F5-III:2, F5-IV:3 and F8-II:4) with AD IRD hallmarked by macular involvement. Prioritization of variants in known IRD genes uncovered a shared, monoallelic *RPE65* variant, c.1555G>A, p.(E519K), initially classified as a variant of unknown significance (VUS). The variant is present in gnomAD v2.1.1 (rs373274945) with an allele frequency of 0.0004014 (allele count: 1, no homozygotes). Subsequently, in-house WES-data from 2,175 individuals with IRD was queried, identifying 28 additional monoallelic p.(E519K) patients (Fig 1).

As their phenotypes often resembled those seen in mitochondrial maculopathy or *ABCA4*-, *BEST1*-, and *PRPH2*-associated maculopathies, an IRD cohort that previously underwent targeted testing for these indications was screened, expanding the p.(E519K) cohort with 14 additional patients. The in-house index patients, identified using this targeted approach, underwent WES to exclude additional (likely) pathogenic variants in IRD genes. Performed genetic analyses and identified variants are listed in Supplementary Table 1. Subsequent segregation analysis revealed 30 clinically affected family members heterozygous for p.(E519K), confirming the dominant inheritance pattern initially established through pedigree analysis (Supplementary Fig 1). Taken together, the Belgian IRD discovery cohort contains 75 monoallelic p.(E519K) cases, all of Flemish origin (in-house cases: *n*=65; external referrals: *n*=10). Furthermore, we expanded our search to other IRD patient cohorts (France, the Netherlands, Germany, United Kingdom [UK], Scotland, Ireland, Canada), representing an IRD replication cohort of 18,796 individuals. Additional monoallelic p.(E519K) IRD cases were identified in the IRD cohorts from France (*n*=3, of which one included in this study), the Netherlands (*n*=1), and Canada (*n*=4, British Columbia; *n*=2, Alberta). To obtain prevalence data in matched controls, we also mined diagnostic non-IRD genomic databases from these regions (overview provided in Supplementary Table 6). Variant p.(E519K) was not found in

347 any of these non-IRD genomic databases collectively representing 136,306 individuals

348 (Supplementary Table 6).

349 A total of 85 monoallelic p.(E519K) individuals with IRD were identified in Belgium, France, the

350 Netherlands, and Canada. This study includes genomic and clinical data from 83/85

351 p.(E519K)-IRD patients, including 48 familial cases, and 35 cases whose families were not

352 available for genetic or clinical investigations.

353

354 *Figure 1. Workflow through which monoallelic patients for RPE65 c.1555G>A p.(E519K) were identified.* *(1-4) represent*

355 *the Belgian IRD discovery cohort: WGS analysis (n=150) and a second step of WES analysis (n=2,175) in IRD cases revealed*

356 *c.1555G>A, p.(E519K) in 3 and 28 cases, respectively. Targeted testing of IRD patient cohorts that tested negative for*

357 *mitochondrial retinopathies (MIDD), ABCA4-, BEST1-, and PRPH2-associated maculopathy (n=518) identified 14 more patients.*

358 *Segregation analysis (n=51) showed segregation of p.(E519K) with disease in 30 affected family members. The total number of*

359 *monoallelic p.(E519K) IRD cases in Belgian discovery cohort: n=75. (5) represents the IRD replication cohort (n=18,796).*

360 *p.(E519K) was mined in IRD registries from France, The Netherlands, Germany, United Kingdom (UK), Scotland, Ireland, Canada.*

361 *The total number of monoallelic p.(E519K) IRD cases found in the replication cohort: n=8, specifically France (n=3; of which one*

362 *included in this study), the Netherlands (n=1), Canada (n=6). Overall number of monoallelic p.(E519K) IRD cases: n=85, of which*

363 *83 are included in this study.*

364 **Index patients with p.(E519K) share a common haplotype of 464 kb**

365 As the majority of IRD cases from the discovery cohort had a reported Flemish origin, a founder

366 effect was suspected. Initial delineation of a common haplotype was performed using long-

367 read WGS on four patients (F5-III:2, F5-IV:3, F8-II:3 and F8-II:4). Established boundaries were

368 used for further haplotype reconstruction using six microsatellite markers flanking *RPE65* in all

369 Belgian (in-house and external) index patients, one of their affected family members (if

370 available), and the French (S34), Dutch (S35) and Canadian (S31) index cases (Fig 2). A

371 minimal shared haplotype of 464 kb between all affected cases was identified, spanning

372 *RPE65* and *DEPDC1*, while the maximal shared region of 1.6 Mb, additionally contains *WLS*,

373 *DIRAS3* and part of *GNG12*. None of these genes, except for *RPE65*, are associated with IRD.

374 Apart from p.(E519K), no other plausible (likely) pathogenic variants were found in the shared
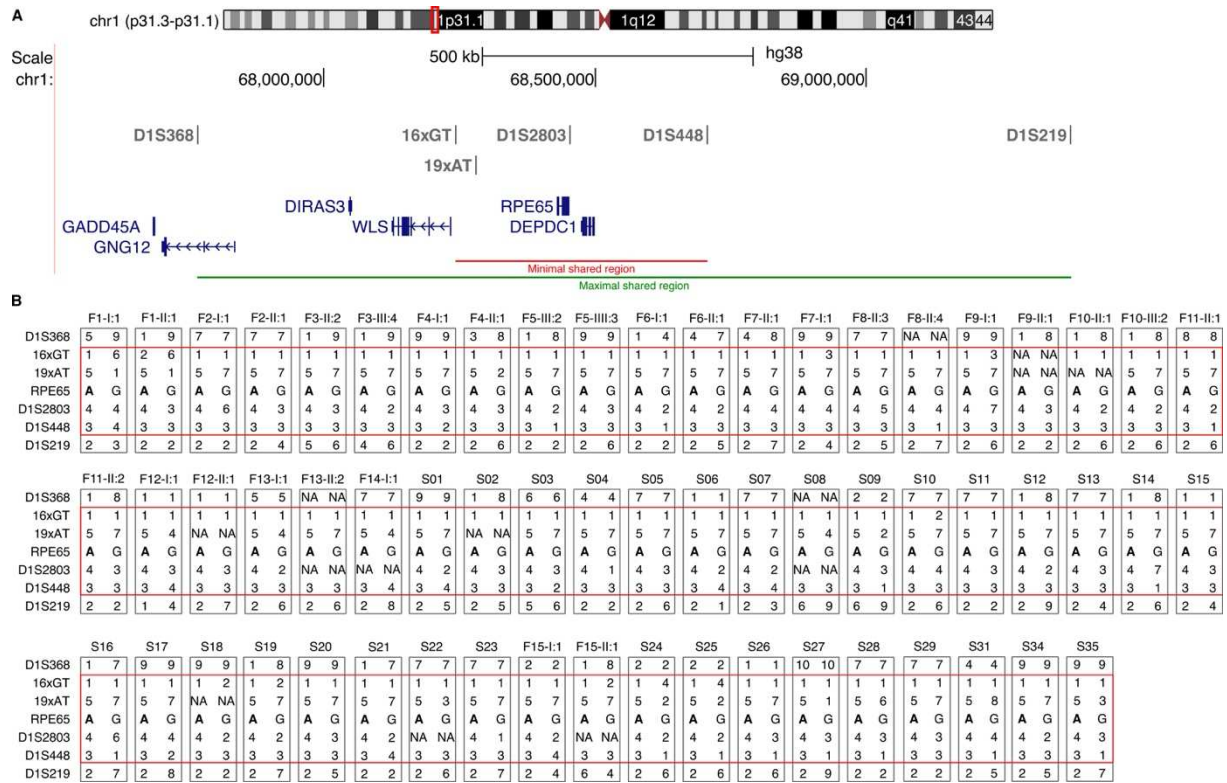
375 region.

376

377 *Figure 2. Haplotype reconstruction in all Belgian index patients, one family member (when available) and the French*

378 *(S34), Dutch (S35) and Canadian (S31) index cases. (A) The location of the six microsatellite markers is depicted above a*

379 *schematic representation of the genes in this region (chr1: 67611911-69469522). Red line: minimal shared region (464 kb), green*

380 *line: maximal shared region (1.6 Mb). (B) Results from haplotype analysis. Each grey box represents the two alleles with the*

381 *patient identifier shown at the top. The c.1555G>A (p.(E519K) variant is indicated in bold and the common allele is shown on the*

382 *left. The red box highlights the shared markers. NA values: missing data. The conversion key for the microsatellite alleles can be*

383 *found in Supplementary Table 9.*

384 ***In silico* and AlphaFold protein modeling supports a destabilizing effect of p.(E519K)**

385 The RPE65 protein is evolutionarily well-conserved, which also applies to Glu[519] and Asp[477]

386 (Fig 3a, Supplementary Fig 2a). When considering their paralogous residues through the wider

387 carotenoid cleavage dioxygenase (CCD) superfamily, of which RPE65 is a member, Glu[519] is

388 conserved in all mammals, and in one of the three zebrafish ohnologs.

389   To assess the potential impact of p.(E519K) and compare its properties with p.(D477G), 24 *in*

390   *silico* predictions were evaluated. Overall, predictions for p.(E519K) compared to p.(D477G)

391   were more damaging or deleterious (Supplementary Table 7). Moreover, Aggrescan predicts

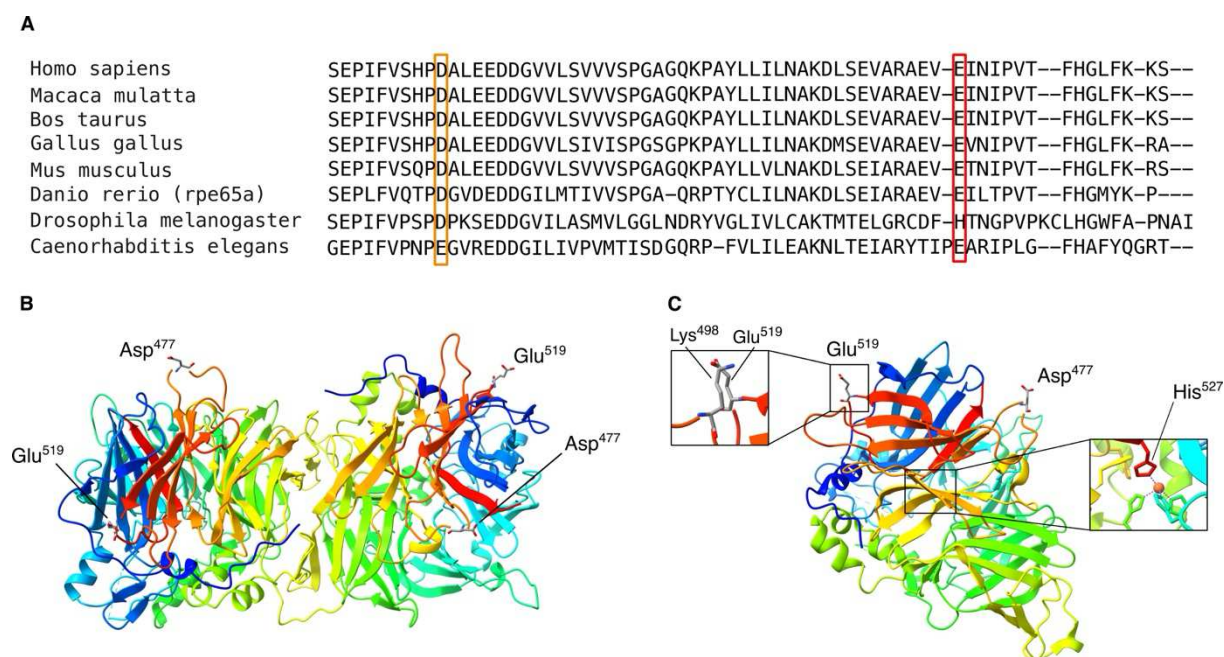392   that both variants are more prone to aggregation compared to WT RPE65 (Supplementary Fig

393   2b-d).

A

```
Homo sapiens            SEPIFVSHPDALEEDDGVVLSVVVSPGAGQKPAYLLILNAKDLSEVARAEV-EINIPVT--FHGLFK-KS--
Macaca mulatta          SEPIFVSHPDALEEDDGVVLSVVVSPGAGQKPAYLLILNAKDLSEVARAEV-EINIPVT--FHGLFK-KS--
Bos taurus              SEPIFVSHPDALEEDDGVVLSVVVSPGAGQKPAYLLILNAKDLSEVARAEV-EINIPVT--FHGLFK-KS--
Gallus gallus           SEPIFVSHPDALEEDDGVVLSIVISPGSGPKPAYLLILNAKDMSEVARAEV-EVNIPVT--FHGLFK-RA--
Mus musculus            SEPIFVSQPDALEEDDGVVLSVVVSPGAGQKPAYLLVLNAKDLSEIARAEV-ETNIPVT--FHGLFK-RS--
Danio rerio (rpe65a)    SEPLFVQTPDGVDEDDGILMTIVVSPGA-QRPTYCLILNAKDLSEIARAEV-EILTPVT--FHGMYK-P---
Drosophila melanogaster SEPIFVPSPDPKSEDDGVILASMVLGGLNDRYVGLIVLCAKTMTELGRCDF-HTNGPVPKCLHGWFA-PNAI
Caenorhabditis elegans  GEPIFVPNPEGVREDDGILIVPVMTISDGQRP-FVLILEAKNLTEIARYTIPEARIPLG--FHAFYQGRT--
```

B

C

394

*Figure 3. Conservation and protein modelling using crystal structures of RPE65. (**A**) The final segment of the amino acid*

alignment for RPE65 of six vertebrate species and the related carotenoid cleavage dioxygenases from two invertebrate species

*is displayed. Orange box: Asp477; red box: Glu519. (**B**) In the 3FSN crystal structure, RPE65 is observed as a dimer. Both Asp477*

*and Glu519 are distant from the dimerization site. (**C**) The monomer crystal structure of RPE65 (4RYX), whereby a positively*

charged lysine (Lys498) is positioned in the vicinity of Glu519. If the glutamate is replaced by a lysine these residues (Lys498 and

Lys519) will repel each other due to their positive charges. His527, important for iron binding in the catalytic center, could be

affected by p.(E519K).

402   Furthermore, crystal structures of RPE65 were examined and AlphaFold models were

403   generated to study the impact of p.(E519K) and p.(D477G) on protein structure and stability.

404   The RPE65 protein exhibits a seven-bladed ß-propeller structure, with Glu^{519} situated on blade

405   VII and Asp^{477} on blade VI (Supplementary Fig 3). Both residues are positioned on the protein's

406   exterior, away from key sites such as the substrate tunnel, water tunnel and the dimerization

407   site (Fig 3b). AlphaFold models for WT-RPE65, p.(E519K) and p.(D477G), in addition to

408   AlphaFold-Multimer modelling, show nearly identical folding and dimer formation, suggesting

409   a minimal impact on protein structure (Supplementary Fig 4). However, based on crystal

410   structures of RPE65 (3FSN; 4RYX), p.(E519K) may induce protein instability due to the

411   proximity of a positively charged Lys[498], causing a repulsion effect with Lys[519] (Fig 3c and

412   Supplementary Fig 4a). Moreover, Glu[519] is located close to His[527] on blade VII, crucial for iron

413   binding in the catalytic center (Fig 3c and Supplementary Fig 3). Consequently, p.(E519K)

414   could indirectly influence enzymatic RPE65 activity. In addition, the electrostatic surface

415   analysis for p.(E519K) shows a shift from a negative to a positive potential at position 519 and

416   the surrounding area (Supplemental Fig 5).

417   **Variant p.(E519K) affects expression, enzymatic activity and thermal stability of RPE65**

418   SpliceAI predicts a potential splicing change for p.(D477G) but not for p.(E519K)

419   (Supplementary Fig 6a). Minigene assays showed aberrant splicing for p.(D477G), including

420   multiple exon skipping events with or without exon 13 skipping (Supplementary Fig 6b,c).

421   Although usage of the strengthened cryptic acceptor site at c.1430 was noted for p.(D477G),

422   this was not increased compared to WT or p.(E519K) (Supplementary Fig 6c). Variant

423   p.(E519K) does not seem to induce an aberrant splicing effect in HEK293-T cells, although a

424   relatively increased ratio of reads containing exon 14 (including 3'UTR) was noted, possibly

425   due to strengthening of the canonical acceptor site of exon 14 (Supplementary Fig 6d).

426   HEK293-T cells were single- or co-transfected with WT-RPE65, p.(D477G) and/or p.(E519K)

427   constructs, followed by immunoblotting. Reduced RPE65 protein expression of p.(D477G) and

428   p.(E519K) compared to WT-RPE65 was found at 59.3% and 49.8%, respectively ($p=0.0016$

429   and $p>0.0001$), following single transfection (Fig 4a,b). Co-expression of WT/p.(D477G) and

430   WT/p.(E519K) did not result in any significant reduction of protein expression ($p>0.9999$ and

431     $p=0.7605$) (Fig 4a,b).

432   Migration of the p.(E519K) protein resembles that of the WT protein, unlike p.(D477G),

433   migrating marginally faster, as previously shown[12]. In addition, we found that p.(E519K)-

434   transfected Expi293 cells produced about 56% of the 11-*cis* retinol compared to WT-RPE65

435   ($p<0.01$) (Fig 4c). Using a CETSA assay the inhibitory concentration (IC_{50}) temperature,

436 whereby 50% of the RPE65 protein is denatured and aggregated, showed a difference

437 between WT, p.(D477G), p.(E519K), WT/p.(D477G) and WT/p.(E519K) (Fig 4e,f and

438 Supplementary Fig 7). Mutant (co-)transfections resulted in an IC_{50} lower than WT

439 (WT/p.(E519K)=47.77°C; WT/p.(D477G)=49.11°C; WT=52.05°C), suggesting p.(D477G) and

440 p.(E519K) result in thermal instability (Fig 4f).

441 Following overexpression experiments in ARPE-19 cells, co-immunoprecipitation showed no

442 (differential) interaction between WT-RPE65 and p.(E519K), in contrast to p.(D477G), which

443 clearly interacts with WT-RPE65 (Fig 4d).
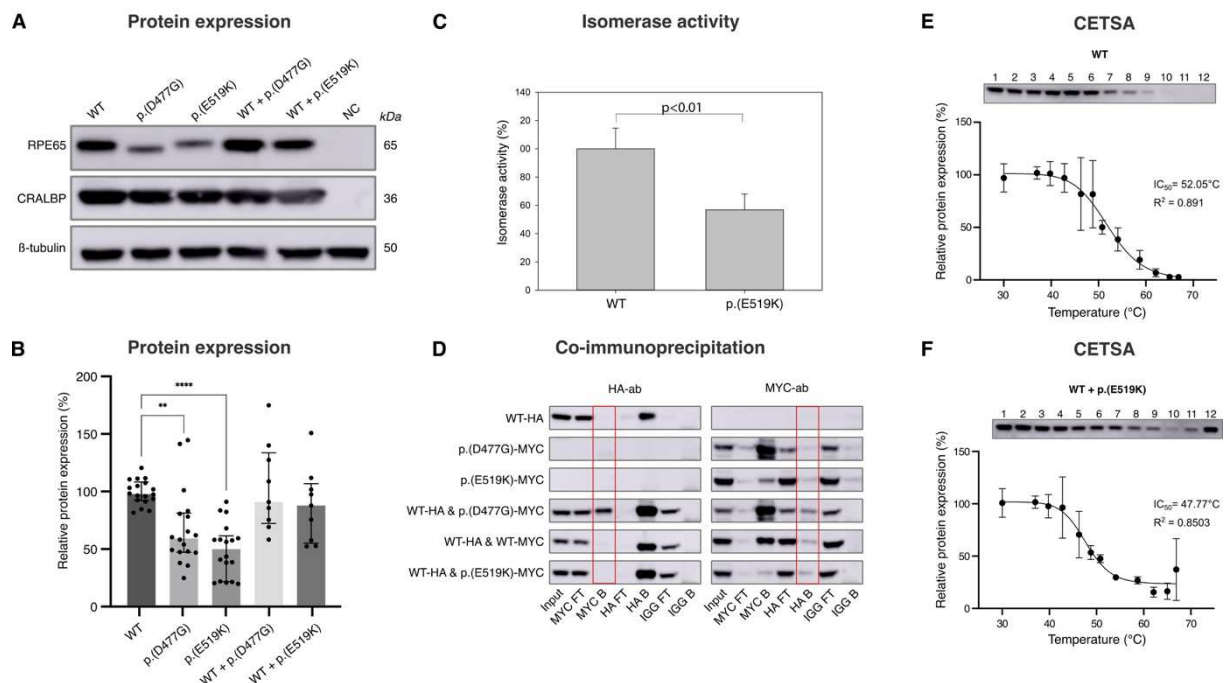

444

445 *Figure 4. Variant p.(E519K) affects expression, enzymatic activity and thermal stability of RPE65. (A) RPE65 protein*

446 *expression following single or co-transfection of vectors encoding WT-RPE, p.(D477G), or p.(E519K) proteins in HEK293-T*

447 *cells. A shift was observed for the p.(D477G) variant. CRALBP and ß-tubulin protein expression were used as transfection and*

448 *loading controls. NTC: no template control. (B) Relative RPE65 protein expression, normalized using CRALBP protein expression,*

449 *is shown. A significant decrease in protein expression is observed after overexpression of p.(D477G) and p.(E519K), compared*

450 *to WT-RPE65. Data are represented as median ± IQR. n = 18 for WT, p.(D477G) and p.(E519K), n=9 for WT+p.(D477G) and*

451 *WT+p.(E519K), * is p<0.05 according to a Kruskal-Wallis test with Dunn's multiple comparisons test. (C) p.(E519K) RPE65*

452 *showed reduced retinol isomerase activity (56%) compared to WT-RPE65 when measured in an in cellulo minimal visual cycle*

453 *assay. (D) In co-IP experiments, ARPE-19 cells were either single or co-transfected with constructs encoding HA-tagged WT-*

454 *RPE65 and/or MYC-tagged p.(D477G) or p.(E519K) protein. Co-IP was performed, using the anti-HA and anti-MYC antibodies*

455 *and western blotting with either anti-HA or anti-MYC antibody was used to determine coprecipitation. The results demonstrate an*

interaction between the D477 and WT-RPE65 proteins, but not between p.(E519K) and WT-RPE65 proteins. Input represents

total protein extract, FT (flow-through) the leftover unbound fraction, and B (bound) proteins specifically bound by the antibodies

*and precipitated by the beads. **(E-F)** Results from a CETSA assay to assess thermal stability after transfection of WT-RPE65 **(E)***

*and co-transfection of WT and p.(E519K) **(F)** in HEK293-T cells. The IC50, the temperature at which 50% of the protein is*

denatured and aggregated, was lowered in the WT + p.(E519K) condition. Immunoblots are depicted above the graphs, labels 1-

12 represent the temperatures at which the cells were incubated (30, 37, 39.8, 42.8, 46.3, 48.8, 50.8, 54.1, 58.7, 62.1, 65.0 and

66.9°C, respectively). A non-linear regression was performed on the data and resulting means with standard deviation are shown

in the graphs. R^2 quantifies goodness of fit.

Comprehensive phenotyping reveals two distinct and recognizable p.(E519K)-IRD phenotypes

An in-depth clinical characterization was performed on 63 in-house patients with AD p.(E519K)-IRD (F1-F14, Supplementary Fig 1). Thirty patients (50.0%) complained of reduced visual acuity and central scotomata (median age at onset 57 years; range 24-76 years) (Table 1 and Supplementary Table 8). The other 30 (50.0%) did not self-report subjective symptoms but showed clinical signs upon ophthalmological investigation (median age at diagnosis 53 years; range 18-74 years) (Table 1 and Supplementary Table 8). BCVA at last exam ranged from 0.01 to 1.00 (median=0.65, interquartile range (IQR)=0.55) in the symptomatic group, and from 0.70 to 1.00 (median=1.00, IQR=0.10) in the asymptomatic group (Supplementary Table 8). Full-field electroretinography in 30 (47.6%) showed predominant rod-system involvement in 14 (46.7%) (Supplementary Table 8).

SW-AF imaging allowed categorization into two distinct phenotypes. A first subgroup of 27 cases (43.5%) was referred to as a 'mottled phenotype' (Fig 5a-e) because of small, diffuse, hypo-autofluorescent (hypo-AF) spots spread over the posterior pole. These usually extended beyond the vascular arcades and the optic nerve head up to the retinal midperiphery. This hypo-AF mottling was often associated with variable hyperautofluorescent (hyper-AF) lesions. The second subgroup was classified as a 'pattern dystrophy', observed in 35 cases (56.5%) and is characterized by more organized hyper-AF changes as predominant feature (Fig 5f-j).
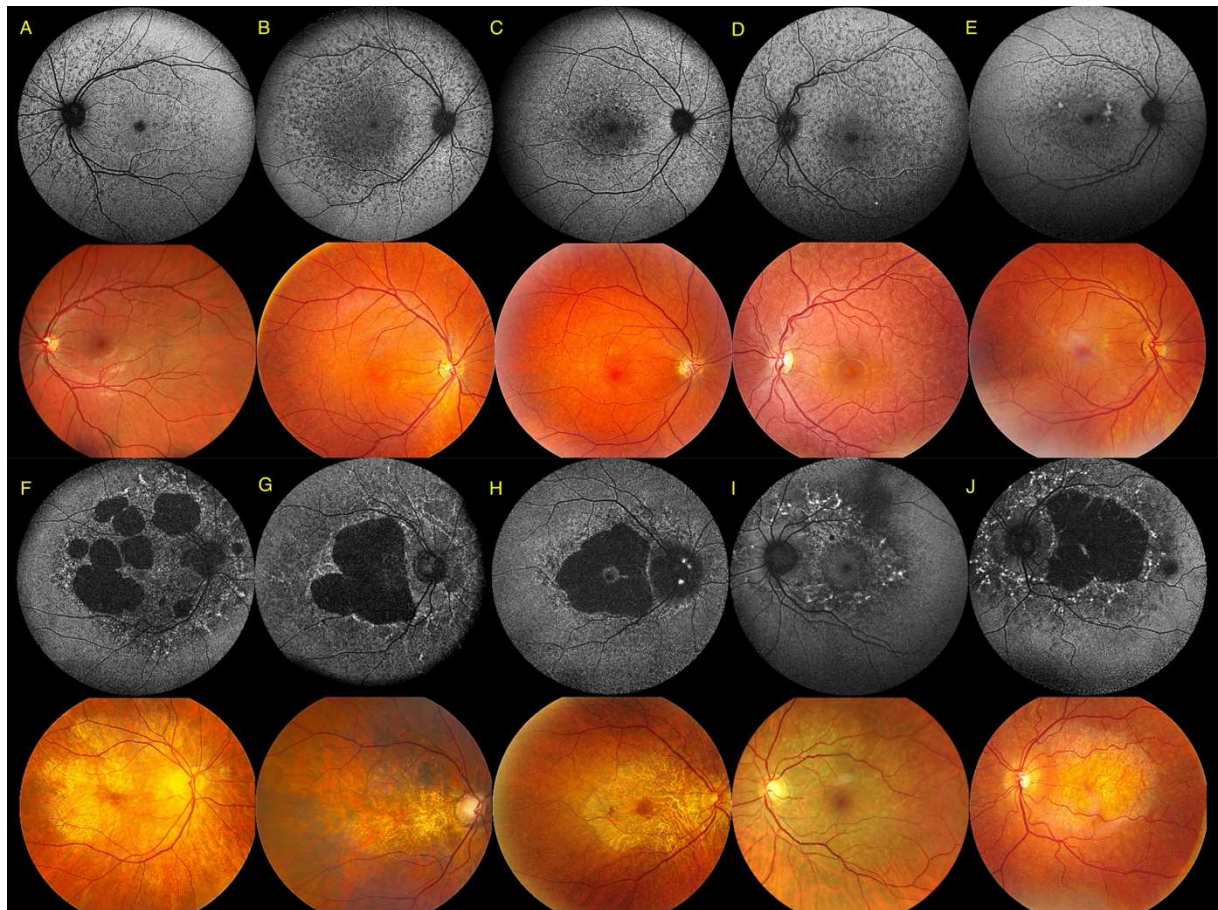
Figure 5. SW-AF imaging (top) and color fundus imaging (bottom) illustrating the representative distinct p.(E519K)-associated phenotypes: mottled phenotype (A-E) and pattern dystrophy (F-J). (A) *Left eye of 31-year-old female (F12-II:1).* **(B)** *Right eye of 41-year-old male (S02).* **(C)** *Right eye of 43-year-old male (F11-II:2).* **(D)** *Left eye of 29-year-old female (F2-III:1).* **(E)** *Right eye of 47-year-old female (F11-II:1).* **(F)** *Right eye of 59-year-old female (S10).* **(G)** *Right eye of 78-year-old male (F4-I:1).* **(H)** *Right eye of 72-year-old female (F3-II:2).* **(I)** *Left eye of 62-year-old female (F5-III:7).* **(J)** *Left eye of 58-year-old male (F8-II:5). SW-AF = short-wavelength autofluorescence.*

Macular chorioretinal atrophic lesions were seen in 55 eyes (44.0%) and associated in all but one eye (S13), with pattern dystrophy. Chorioretinal atrophy was either bilateral (22; 68.8%) or unilateral (10; 31.3%) (Supplementary Table 8). Although an extensive variability was noted in the p.(E519K) cohort (Supplemental Fig 10), lower visual acuities and larger surface areas of chorioretinal atrophy tended to be associated with older age.

Color fundus images often showed subtle changes compared to SW-AF imaging (Fig 5). Unifocal vitelliform lesions were observed in 11 eyes (8.8%), at the fovea (Supplementary Fig 11). Electro-oculography in four of these six cases showed two cases with mildly subnormal light peak-to-dark trough ratios (1.7-1.8). Cystoid macular edema was observed in 15 eyes

499   (12.0%), seven of which had a vitelliform lesion. Structural retinal layer abnormalities were

500   primarily located at the three outermost hyperreflective bands on OCT. The innermost of these,

501   the ellipsoid zone (EZ), often showed a fine sinusoidal deformation. More severe EZ alterations

502   were observed, often in older eyes. Lesions hyper-AF on SW-AF imaging appeared as

503   hyperreflective, tall, smooth, bell-shaped lesions or as wider-than-tall lesions with an irregular

504   surface arising from the hyperreflective band corresponding to the RPE-Bruch membrane

505   complex. Chorioretinal atrophic lesions often showed degenerative intraretinal cavitation and

506   outer retinal tubulations (Supplementary Fig 12). The phenotypes observed in patients referred

507   by external experts (S22-S35, F15-I:1, F15-II:1, F16-II:1, F16-II:2) are indistinguishable from

508   those seen in the in-house IRD cohort (Supplementary Fig 13). Several particular phenotypes

509   were found in our overall p.(E519K)-IRD cohort. Two patients (F10-II:1 and S20) had been

510   considered molecularly solved due to biallelic pathogenic *ZNF408* and *CEP290* variants. Their

511   severe early-onset IRD had masked the p.(E519K)-IRD (Supplementary Figures 8 and 9). For

512   this reason, these patients were excluded from the aforementioned clinical analyses. Another

513   outlier is S22, displaying a retinitis pigmentosa-type rod-cone dystrophy (RCD). No other

514   coding (likely) pathogenic variants that could explain the RCD were identified using WES

515   (Supplementary Fig 14).

Discussion

We present and characterize *RPE65* variant p.(E519K) as a novel cause of dominant IRD, often manifesting as an adult-onset maculopathy. The common haplotype of 464 kb was shared by all monoallelic cases of the discovery cohort and by the index cases of the replication cohort, supporting a founder effect. The geographical background of the Belgian cases suggests a Flemish origin of p.(E519K). Hence, the presence of p.(E519K) in IRD patients from regions where Flemish people migrated to, specifically France, the Netherlands and Canada, is not surprising. Its overall rarity in gnomAD v2.1.1 as well as in the other genomic databases we mined emphasizes the importance of increasing genetic ancestral diversity in population-scale datasets[60].

The fact that another *RPE65* variant has been reported at the same location, c.1555G>T, p.(Glu519Ter), in the context of AR *RPE65*-IRD, suggests this guanine is prone to variation[61]. *In silico* predictions and (dimer) protein modelling support a deleterious effect of p.(E519K) even stronger than for p.(D477G). Protein instability of p.(E519K) can be explained by a repulsion effect between Lys[519] and Lys[498], the shift in surface potential, as well as a potential destabilising effect on His[527], essential for iron binding in the catalytic centre. Moreover, a significantly reduced protein expression as well as reduced isomerase enzymatic activity of p.(E519K) compared to WT was demonstrated, similar to p.(D477G)[16,17]. Pure loss-of-function (LOF) is unlikely to be the only effect, as heterozygous carriers of *RPE65* LOF variants exhibit no phenotype. However, a larger cell type-specific LOF effect might not be captured *in vitro*. Moreover, both the thermal instability induced by p.(E519K), together with an increased aggregation hot spot, support that p.(E519K) is prone to aggregation, a known effect of p.(D477G) and of variants in other IRD genes[17,62,63]. While we confirmed the known interaction between p.(D477G) and WT-RPE65[17], no interaction was observed between p.(E519K) and WT-RPE65, making a dominant-negative effect in this cell type less likely. Although aberrant splicing had been demonstrated for p.(D477G)[16], we could not demonstrate a strong effect on

splicing for p.(E519K), also supported by SpliceAI. However, a cell type-specific splicing effect in patient-derived RPE cells cannot be excluded, as splicing is highly cell-type specific [15–17,64–68].

Several knock-in p.(D477G) mice (both WT/KI and KI/KI) have been generated, of which the phenotypes were highly variable and dependent on age, luminescence exposure and genetic background[15,16,65,66,69]. These mice lacked a discernible phenotype and thus did not accurately recapitulate the human situation. More biologically relevant models, such as patient-derived induced pluripotent stem cell (iPSC)-retinal pigment epithelium (RPE) (iPSC-RPE), mimic the native conditions of RPE65, including its native splicing, expression, localisation and interactions patterns, and will contribute to understanding the pathomechanisms of p.(E519K)- and p.(D477G)-IRD.

In addition, an extensive clinical characterization of the 63 Belgian p.(E519K)-IRD patients revealed two distinct phenotypic subtypes. The hypo-AF mottled subtype (43.5%) is characterized by small, diffuse, hypo-AF spots spread out across the posterior pole. This phenotype seems pathognomonic for this novel AD *RPE65*-IRD and could guide towards its molecular diagnosis. A second predominant subtype (56.5%) displays a pattern dystrophy most often resembling the mitochondrial retinopathy due to *MT-TL1* m.3243A>G[70]. We hypothesize that the mottled phenotype might evolve into the more severe pattern dystrophy over time, representing the milder and more severe end of the p.(E519K)-IRD phenotypic spectrum, respectively. Long-term follow-up of affected individuals will be useful to support this. Lower visual acuity and larger surface area of chorioretinal atrophy were associated with older age, while variability in disease severity was observed in the patient cohort (Supplementary Fig 10). Overall, this differs from the severe rod-cone dystrophy associated with AR *RPE65*-IRD[6,71,72] and the p.(D477G)-IRD that was initially described as an adult-onset choroideremia-like IRD with reduced or non-penetrance[12].

567 Familial co-segregation analysis showed that all cases that are monoallelic for p.(E519K)

568 displayed clinical signs upon retinal evaluation, albeit sometimes subtle and often not

569 associated with subjective visual symptoms.

570 In the differential diagnosis of the p.(E519K) pattern dystrophy phenotype, mitochondrial

571 retinopathies, *ABCA4*-IRD and *PRPH2*-IRD can be considered. Multiple atrophic lesions in

572 patients above 50 years could be misdiagnosed as geographic atrophy in dry age-related

573 macular degeneration (AMD). However, the additional pattern dystrophy on SW-AF imaging is

574 different from AMD. For those patients in whom vitelliform lesions are predominant, other AD

575 IRD caused by monoallelic variants in *BEST1*, *IMPG1*, *IMPG2* and *PRPH2* need to be

576 considered.

577 Given the approved *RPE65* gene augmentation therapy *Voretigene neparvovec-rzyl*

578 (Luxturna®) for patients with AR *RPE65*-IRD, unravelling the pathomechanisms of AD *RPE65*-

579 IRD is thus of utmost importance in view of potential treatment options. For AD p.(D477G)-IRD

580 gene augmentation therapy has been performed in a p.(D477G) KI murine model, resulting in

581 improved retinal function[69]. Moreover, oral 9-*cis* retinyl acetate therapy has been administered

582 to five p.(D477G) patients, three of whom displayed improved visual function[69,73]. However,

583 the long-term effects of either of these approaches on mutant toxicity and retinal degeneration

584 are not yet known. Gene augmentation therapy would only prove beneficial when the

585 mechanism of action includes LOF including haploinsufficiency. As mentioned, these

586 mechanisms alone are unlikely to cause AD *RPE65*-IRD as carriers of recessive LOF variants

587 show no clinical signs. A gain-of-function or dominant-negative effect combined or not with a

588 LOF seem more plausible pathomechanisms. In such scenarios, augmentation therapy could

589 induce toxic effects[74,75]. A potential therapy could involve antisense oligonucleotides (ASOs)

590 to specifically target and degrade the mutant allele. Proof-of-principle studies using ASOs have

591 been performed for several IRD genes, for example *RHO*[76]. Gene editing, including

592 CRISPR/Cas9-based or prime editing[77,78], is another therapeutic option for this variant. This

593 would allow to permanently correct the mutation, illustrated by EDIT-101, targeting the *CEP290*

594   IVS26 variant (NCT03872479) [79,80]. As a gene therapy approach for a dominant IRD is guided

595   by its underlying mechanism, further research into its pathogenesis is needed.

596   Comprehensive genetic testing is key to establishing an early diagnosis in suspected

597   p.(E519K)-IRD, which is crucial to provide adequate counselling and will only gain importance

598   as therapies for this and similar retinal disorders will become available.

599   Conclusions

600   Our study provides strong genetic, clinical, molecular and functional evidence for a novel,

601   adult-onset dominant *RPE65*-associated retinopathy due to founder variant p.(E519K). These

602   findings substantially expand the spectrum of *RPE65*-IRD, reduce the diagnostic gap in

603   dominant IRD, and open potential new therapeutic perspectives for AD *RPE65*-IRD.

Authors' contributions

These first authors contributed equally: Eline Van Vooren, Filip Van den Broeck.

These last authors contributed equally: Julie De Zaeytijd, Bart P. Leroy, Miriam Bauwens and

Elfride De Baere.

EVV: Conceptualization, Data curation, Formal analysis, Investigation, Methodology, Project

administration, Validation, Visualization, Writing – original draft and Writing – review & editing

FVB: Conceptualization, Data curation, Formal analysis, Investigation, Methodology, Project

administration, Validation, Visualization, Writing – original draft and Writing – review &editing.

Q.M: Investigation and Formal analysis.

E.G.: Investigation and Formal analysis.

M.V.H.: Data curation, Investigation, Formal analysis and Software

M.D.B.: Investigation, Formal analysis and Validation.

S.V.S.: Investigation, Formal analysis and Validation.

S.U.: Investigation and Formal analysis.

E.P.: Investigation and Formal analysis.

C.-M.D.: Investigation and Resources.

C.Y.G.-E.: Investigation and Resources.

L.H.: Investigation and Resources.

A.I.G.: Investigation and Resources.

S.K.: Investigation, Resources and Writing – review & editing.

T.Z.: Investigation and Resources.

T.D.: Investigation and Resources.

Dominant RPE65-p.(E519K) Consortium: Formal analysis (data mining).

S.T.: Investigation and Resources.

J.R.: Investigation and Resources.

L.V.O.: Investigation and Resources.

630   E.P.: Investigation and Resources.

631   J.J.: Investigation and Resources.

632   S.V.: Investigation and Resources.

633   L.P.: Investigation and Resources.

634   K.D.: Investigation and Resources.

635   I.M.: Investigation and Resources.

636   F.R.: Investigation and Resources.

637   A.A.H.J.T.: Investigation and Resources.

638   K.A.J.S.: Investigation and Resources.

639   N.S.: Investigation and Resources.

640   V.S.: Investigation and Resources.

641   I.M.M.: Investigation and Resources.

642   K.G.-E.: Investigation and Resources.

643   T.M.R.: Formal analysis, Investigation, Resources, Project administration and Writing –

644   review & editing.

645   J.D.Z.: Conceptualization, Investigation, Project administration, Resources, Supervision,

646   Validation, and Writing – review & editing.

647   B.P.L.: Conceptualization, Funding acquisition, Investigation, Project administration,

648   Resources, Supervision, Validation, and Writing – review & editing.

649   M.B.: Conceptualization, Funding acquisition, Investigation, Project administration,

650   Resources, Supervision, Validation, and Writing – review & editing.

651   E.D.B.: Conceptualization, Funding acquisition, Investigation, Project administration,

652   Resources, Supervision, Validation, and Writing – review & editing.

653

654   **Conflicts of Interests**

655   The authors declare no competing interests

Dominant RPE65-p.(E519K) Consortium

Lonneke Haer-Wigman, Susanne Roosing, Department of Human Genetics, Radboud

University Medical Center, Nijmegen, The Netherlands.

Andrew R. Webster, Siying Lin, Gavin Arno, Omar Mahroo, National Institute of Health

Research Biomedical Research Centre at Moorfields Eye Hospital and the UCL Institute of

Ophthalmology, London, UK.

Roly Megaw, MRC Human Genetics Unit, MRC Institute of Genetics & Cancer, University of

Edinburgh, Western General Hospital, Edinburgh, EH4 2XU, UK & Princess Alexandra Eye

Pavilion, NHS Lothian, Chalmers St, Edinburgh, EH3 9HA, UK

Mihail Halachev, MRC Human Genetics Unit, MRC Institute of Genetics & Cancer, University

of Edinburgh, Western General Hospital, Edinburgh, EH4 2XU, UK

Anne Lampe, South East of Scotland Clinical Genetics Service, Western General Hospital,

Edinburgh, UK.

David Gilmour, Gartnavel Hospital, NHS Greater Glasgow and Clyde, Great Western Rd,

Glasgow G12 0YN, UK

681   Andreea Ionean, Aberdeen Royal Infirmary, NHS Grampian, Forresterhill Road, Aberdeen,

682   AB25 2ZN, UK

683   Nick George, Ninewells Hospital, NHS Tayside, James Arrott Dr, Dundee, DD2 1SG, UK

684   Adrian Dockery, Mater Misericordiae University Hospital, Dublin, Ireland.

685   Laura Finnegan, G. Jane Farrar, School of Genetics & Microbiology, Trinity College Dublin,

686   Ireland.

References

688   1.   Bourne RRA, Steinmetz JD, Saylan M, et al. Causes of blindness and vision
689   impairment in 2020 and trends over 30 years, and prevalence of avoidable
690   blindness in relation to VISION 2020: The Right to Sight: An analysis for the Global
691   Burden of Disease Study. *Lancet Glob Health*. 2021;9(2):e144-e160.
692   doi:10.1016/S2214-109X(20)30489-7
693   2.   WHO. Blindness and vision impairment. August 10, 2023. Accessed October 1,
694   2023. https://www.who.int/news-room/fact-sheets/detail/blindness-and-visual-
695   impairment
696   3.   Redmond. TM, Yu S, Lee E, et al. Rpe65 is necessary for production of 11-cis-
697   vitamin A in the retinal visual cycle. *Nat Genet*. 1998;20(4):344-351.
698   doi:10.1038/3813
699   4.   Redmond TM, Poliakov E, Yu S, Tsai JY, Lu Z, Gentleman S. Mutation of key
700   residues of RPE65 abolishes its enzymatic role as isomerohydrolase in the visual
701   cycle. *Proc Natl Acad Sci U S A*. 2005;102(38):13658-13663.
702   doi:10.1073/pnas.0504167102
703   5.   Moiseyev G, Chen Y, Takahashi Y, Wu BX, Ma JX. *RPE65 Is the Isomerohydrolase in*
704   *the Retinoid Visual Cycle*.; 2005. www.pnas.orgcgidoi10.1073pnas.0503460102
705   6.   Chung DC, Bertelsen M, Lorenz B, et al. The Natural History of Inherited Retinal
706   Dystrophy Due to Biallelic Mutations in the RPE65 Gene. *Am J Ophthalmol*.
707   2019;199:58-70. doi:10.1016/j.ajo.2018.09.024
708   7.   Ciulla TA, Hussain RM, Berrocal AM, Nagiel A. Voretigene neparvovec-rzyl for
709   treatment of RPE65-mediated inherited retinal diseases: a model for ocular gene
710   therapy development. *Expert Opin Biol Ther*. 2020;20(6):565-578.
711   doi:10.1080/14712598.2020.1740676
712   8.   Maguire A, Russell S, Chung D, et al. Durability of Voretigene Neparvovec for
713   Biallelic RPE65-Mediated Inherited Retinal Disease: Phase 3 Results at 3 Years
714   and 4 Years. *Ophthalmology*. 2021;128. doi:10.1016/j.ophtha.2021.03.031
715   9.   Maguire AM, Russell S, Wellman JA, et al. Efficacy, Safety, and Durability of
716   Voretigene Neparvovec-rzyl in RPE65 Mutation–Associated Inherited Retinal
717   Dystrophy: Results of Phase 1 and 3 Trials. *Ophthalmology*. 2019;126(9):1273-
718   1285. doi:https://doi.org/10.1016/j.ophtha.2019.06.017
719   10.   Russell S, Bennett J, Wellman JA, et al. Efficacy and safety of voretigene
720   neparvovec (AAV2-hRPE65v2) in patients with RPE65-mediated inherited retinal
721   dystrophy: a randomised, controlled, open-label, phase 3 trial. *Lancet*.
722   2017;390(10097):849-860. doi:10.1016/S0140-6736(17)31868-8

723 11. Hull S, Mukherjee R, Holder GE, Moore AT, Webster AR. The clinical features of
724 retinal disease due to a dominant mutation in RPE65. *Mol Vis*. 2016;22:626-635.

725 12. Bowne SJ, Humphries MM, Sullivan LS, et al. A dominant mutation in RPE65
726 identified by whole-exome sequencing causes retinitis pigmentosa with choroidal
727 involvement. *Eur J Hum Genet*. 2011;19(10):1074-1081. doi:10.1038/ejhg.2011.86

728 13. Jauregui R, Park KS, Tsang SH. Two-year progression analysis of RPE65 autosomal
729 dominant retinitis pigmentosa. *Ophthalmic Genet*. 2018;39(4):544-549.
730 doi:10.1080/13816810.2018.1484929

731 14. Jauregui R, Cho A, Oh JK, Tanaka AJ, Sparrow JR, Tsang SH. Phenotypic expansion
732 of autosomal dominant retinitis pigmentosa associated with the D477G mutation
733 in RPE65. *Cold Spring Harb Mol Case Stud*. 2020;6(1). doi:10.1101/mcs.a004952

734 15. Choi EH, Suh S, Sander CL, et al. Insights into the pathogenesis of dominant
735 retinitis pigmentosa associated with a D477G mutation in RPE65. *Hum Mol Genet*.
736 2018;27(13):2225-2243. doi:10.1093/hmg/ddy128

737 16. Li Y, Furhang R, Ray A, et al. Aberrant RNA splicing is the major pathogenic effect
738 in a knock-in mouse model of the dominantly inherited c.1430A>G human RPE65
739 mutation. *Hum Mutat*. 2019;40(4):426-443. doi:10.1002/humu.23706

740 17. Wu W, Takahashi Y, Younghwa Shin H, et al. The interplay of environmental
741 luminance and genetics in the retinal dystrophy induced by the dominant RPE65
742 mutation. Published online 2022. doi:10.1073/pnas

743 18. Lange C, Feltgen N, Junker B, Schulze-Bonsel K, Bach M. Resolving the clinical
744 acuity categories "hand motion" and "counting fingers" using the Freiburg Visual
745 Acuity Test (FrACT). *Graefe's Archive for Clinical and Experimental*
746 *Ophthalmology*. 2009;247(1):137-142. doi:10.1007/s00417-008-0926-0

747 19. Illumina. bcl2fastq2 Conversion Software v2.20.
748 https://emea.support.illumina.com/downloads/bcl2fastq-conversion-software-
749 v2-20.html.

750 20. lh3 / bwa. https://github.com/lh3/bwa.

751 21. Poplin R, Ruano-Rubio V, DePristo MA, et al. Scaling accurate genetic variant
752 discovery to tens of thousands of samples. *bioRxiv*. Published online January 1,
753 2018:201178. doi:10.1101/201178

754 22. McLaren W, Gil L, Hunt SE, et al. The Ensembl Variant Effect Predictor. *Genome*
755 *Biol*. 2016;17(1). doi:10.1186/s13059-016-0974-4

756 23. Liu X, Li C, Mou C, Dong Y, Tu Y. dbNSFP v4: a comprehensive database of
757 transcript-specific functional predictions and annotations for human
758 nonsynonymous and splice-site SNVs. *Genome Med*. 2020;12(1).
759 doi:10.1186/s13073-020-00803-9

760 24. bcbio-nextgen. https://github.com/bcbio/bcbio-nextgen.

761 25. Chen X, Schulz-Trieglaff O, Shaw R, et al. Manta: Rapid detection of structural
762 variants and indels for germline and cancer sequencing applications.
763 *Bioinformatics*. 2016;32(8):1220-1222. doi:10.1093/bioinformatics/btv710

764 26. Rausch T, Zichner T, Schlattl A, Stütz AM, Benes V, Korbel JO. DELLY: Structural
765 variant discovery by integrated paired-end and split-read analysis. *Bioinformatics*.
766 2012;28(18). doi:10.1093/bioinformatics/bts378

767 27. Ellard S, Baple EL, Callaway A, et al. ACGS Best Practice Guidelines for Variant
768 Classification in Rare Disease 2020 Recommendations ratified by ACGS Quality
769 Subcommittee on 4 th. Published online 2020. doi:10.1101/531210

770　28.　Biesecker LG, Harrison SM. The ACMG/AMP reputable source criteria for the
771　　　interpretation of sequence variants. *Genet Med*. 2018;20(12):1687-1688.
772　　　doi:10.1038/GIM.2018.42
773　29.　Abou Tayoun AN, Pesaran T, DiStefano MT, et al. Recommendations for
774　　　interpreting the loss of function PVS1 ACMG/AMP variant criterion. *Hum Mutat*.
775　　　2018;39(11):1517-1524. doi:10.1002/HUMU.23626
776　30.　Nykamp K, Anderson M, Powers M, et al. Sherloc: a comprehensive refinement of
777　　　the ACMG-AMP variant classification criteria. *Genet Med*. 2017;19(10):1105-1117.
778　　　doi:10.1038/GIM.2017.37
779　31.　Richards S, Aziz N, Bale S, et al. Standards and guidelines for the interpretation of
780　　　sequence variants: a joint consensus recommendation of the American College
781　　　of Medical Genetics and Genomics and the Association for Molecular Pathology.
782　　　*Genet Med*. 2015;17(5):405-424. doi:10.1038/GIM.2015.30
783　32.　Plagnol V, Curtis J, Epstein M, et al. A robust model for read count data in exome
784　　　sequencing experiments and implications for copy number variant calling.
785　　　*Bioinformatics*. 2012;28(21):2747-2754. doi:10.1093/bioinformatics/bts526
786　33.　Blueprint genetics. Retinal Dystrophy Panel.
787　　　https://blueprintgenetics.com/tests/panels/ophthalmology/retinal-dystrophy-
788　　　panel/. Accessed June 1, 2024.
789　　　https://blueprintgenetics.com/tests/panels/ophthalmology/retinal-dystrophy-
790　　　panel/
791　34.　Invitae. Invitae Inherited Retinal Disorders Panel.
792　　　https://www.invitae.com/us/providers/test-catalog/test-72100. Accessed June 2,
793　　　2024. https://www.invitae.com/us/providers/test-catalog/test-72100
794　35.　Khan M, Cornelis SS, Pozo-Valero MD, et al. Resolving the dark matter of ABCA4
795　　　for 1054 Stargardt disease probands through integrated genomics and
796　　　transcriptomics. *Genet Med*. 2020;22(7):1235-1246. doi:10.1038/s41436-020-
797　　　0787-4
798　36.　Li H. Minimap2: Pairwise alignment for nucleotide sequences. *Bioinformatics*.
799　　　2018;34(18):3094-3100. doi:10.1093/bioinformatics/bty191
800　37.　Heller D, Vingron M. SVIM: Structural variant identification using mapped long
801　　　reads. *Bioinformatics*. 2019;35(17):2907-2915.
802　　　doi:10.1093/bioinformatics/btz041
803　38.　Smolka M, Paulin LF, Grochowski CM, et al. Detection of mosaic and population-
804　　　level structural variants with Sniffles2. *Nat Biotechnol*. Published online 2024.
805　　　doi:10.1038/s41587-023-02024-y
806　39.　Jiang T, Liu Y, Jiang Y, et al. Long-read-based human genomic structural variation
807　　　detection with cuteSV. *Genome Biol*. 2020;21(1). doi:10.1186/s13059-020-02107-
808　　　y
809　40.　mkirsche. Jasmine. https://github.com/mkirsche/Jasmine.
810　41.　Zheng Z, Li S, Su J, Leung AWS, Lam TW, Luo R. Symphonizing pileup and full-
811　　　alignment for deep learning-based long-read variant calling. *Nat Comput Sci*.
812　　　2022;2(12):797-803. doi:10.1038/s43588-022-00387-x
813　42.　Martin M, Patterson M, Garg S, et al. WhatsHap: fast and accurate read-based
814　　　phasing. *bioRxiv*. Published online January 1, 2016:085050. doi:10.1101/085050
815　43.　Pedersen BS, Quinlan AR. Mosdepth: Quick coverage calculation for genomes and
816　　　exomes. *Bioinformatics*. 2018;34(5):867-868. doi:10.1093/bioinformatics/btx699

817   44.   Leger Adrien, Leonardi Tommaso. pycoQC. https://github.com/a-slide/pycoQC.

818   45.   De Coster W, D'Hert S, Schultz DT, Cruts M, Van Broeckhoven C. NanoPack:
819   Visualizing and processing long-read sequencing data. *Bioinformatics*.
820   2018;34(15):2666-2669. doi:10.1093/bioinformatics/bty149

821   46.   Redmond TM, Poliakov E, Kuo S, Chander P, Gentleman S. RPE65, visual cycle
822   retinol isomerase, is not inherently 11-cis-specific: Support for a carbocation
823   mechanism of retinol isomerization. *Journal of Biological Chemistry*.
824   2010;285(3):1919-1927. doi:10.1074/jbc.M109.027458

825   47.   Landers GM, Olson JA. Rapid, simultaneous determination of isomers of retinal,
826   retinal oxime and retinol by high. *J Chromatogr A*. 1988;438(2):383-392.
827   doi:10.1016/s0021-9673(00)90269-3

828   48.   Dobin A, Davis CA, Schlesinger F, et al. STAR: Ultrafast universal RNA-seq aligner.
829   *Bioinformatics*. 2013;29(1):15-21. doi:10.1093/bioinformatics/bts635

830   49.   Danecek P, Bonfield JK, Liddle J, et al. Twelve years of SAMtools and BCFtools.
831   *Gigascience*. 2021;10(2). doi:10.1093/gigascience/giab008

832   50.   Jumper J, Evans R, Pritzel A, et al. Highly accurate protein structure prediction
833   with AlphaFold. *Nature*. 2021;596:583. doi:10.1038/s41586-021-03819-2

834   51.   Kiser PD, Golczak M, Lodowski DT, Chance MR, Palczewski K. *Crystal Structure of*
835   *Native RPE65, the Retinoid Isomerase of the Visual Cycle*.; 2009.
836   www.pnas.orgcgidoi10.1073pnas.0906600106

837   52.   Zhang J, Kiser PD, Badiee M, et al. Molecular pharmacodynamics of emixustat in
838   protection against retinal degeneration. *Journal of Clinical Investigation*.
839   2015;125(7):2781-2794. doi:10.1172/JCI80950

840   53.   Liu X, Li C, Mou C, Dong Y, Tu Y. dbNSFP v4: a comprehensive database of
841   transcript-specific functional predictions and annotations for human
842   nonsynonymous and splice-site SNVs. *Genome Med*. 2020;12(1).
843   doi:10.1186/s13073-020-00803-9

844   54.   Adzhubei IA, Schmidt S, Peshkin L, et al. A method and server for predicting
845   damaging missense mutations. *Nat Methods*. 2010;7(4):248-249.
846   doi:10.1038/nmeth0410-248

847   55.   Steinhaus R, Proft S, Schuelke M, Cooper DN, Schwarz JM, Seelow D.
848   MutationTaster2021. *Nucleic Acids Res*. 2021;49. doi:10.1093/nar/gkab266

849   56.   Quinodoz M, Peter VG, Cisarova K, et al. Analysis of missense variants in the
850   human genome reveals widespread gene-specific clustering and improves
851   prediction of pathogenicity. *Am J Hum Genet*. 2022;109(3):457-470.
852   doi:10.1016/j.ajhg.2022.01.006

853   57.   Cheng J, Novati G, Pan J, et al. Accurate proteome-wide missense variant effect
854   prediction with AlphaMissense. *Science (1979)*. 2023;381(6664).
855   doi:10.1126/science.adg7492

856   58.   SpliceAI Lookup. https://spliceailookup.broadinstitute.org.

857   59.   Conchillo-Solé O, de Groot NS, Avilés FX, Vendrell J, Daura X, Ventura S.
858   AGGRESCAN: A server for the prediction and evaluation of "hot spots" of
859   aggregation in polypeptides. *BMC Bioinformatics*. 2007;8. doi:10.1186/1471-
860   2105-8-65

861   60.   Chen S, Francioli LC, Goodrich JK, et al. A genomic mutational constraint map
862   using variation in 76,156 human genomes. | *Nature* |. 2024;625.
863   doi:10.1038/s41586-023-06045-0

864 61. Testa F, Murro V, Signorini S, et al. RPE65-Associated Retinopathies in the Italian
865   Population: A Longitudinal Natural History Study. *Invest Ophthalmol Vis Sci*.
866   2022;63(2). doi:10.1167/iovs.63.2.13

867 62. Vasudevan S, Senapati S, Pendergast M, Park PS –H. Aggregation of rhodopsin
868   mutants in mouse models of autosomal dominant retinitis pigmentosa. *Nat*
869   *Commun*. 2024;15(1). doi:10.1038/s41467-024-45748-4

870 63. Valdés-Sánchez L, Calado SM, De La Cerda B, et al. Retinal pigment epithelium
871   degeneration caused by aggregation of PRPF31 and the role of HSP70 family of
872   proteins. *Molecular Medicine*. 2019;26(1). doi:10.1186/s10020-019-0124-z

873 64. Lu Y, Shiau F, Yi W, et al. Single-Cell Analysis of Human Retina Identifies
874   Evolutionarily Conserved and Species-Specific Mechanisms Controlling
875   Development. *Dev Cell*. 2020;53(4):473-491.e9.
876   doi:https://doi.org/10.1016/j.devcel.2020.04.009

877 65. Shin Y, Moiseyev G, Chakraborty D, Ma J xing. A Dominant Mutation in Rpe65,
878   D477G, Delays Dark Adaptation and Disturbs the Visual Cycle in the Mutant
879   Knock-In Mice. *American Journal of Pathology*. 2017;187(3):517-527.
880   doi:10.1016/j.ajpath.2016.11.004

881 66. Kiang AS, Kenna PF, Humphries MM, et al. Properties and Therapeutic
882   Implications of an Enigmatic D477G RPE65 Variant Associated with Autosomal
883   Dominant Retinitis Pigmentosa. *Genes (Basel)*. 2020;11.
884   doi:10.3390/genes11121420

885 67. Garanto A, van Beersum SE, Peters TA, Roepman R, Cremers FP, Collin RW.
886   Unexpected CEP290 mRNA splicing in a humanized knock-in mouse model for
887   Leber congenital amaurosis. *PLoS One*. 2013;8(11):e79369.
888   doi:10.1371/journal.pone.0079369

889 68. Sangermano R, Bax NM, Bauwens M, et al. Photoreceptor Progenitor mRNA
890   Analysis Reveals Exon Skipping Resulting from the ABCA4 c.5461-10T→C Mutation
891   in Stargardt Disease. *Ophthalmology*. 2016;123(6):1375-1385.
892   doi:10.1016/j.ophtha.2016.01.053

893 69. Feathers KL, Jia L, Khan NW, et al. Gene Supplementation in Mice Heterozygous
894   for the D477G RPE65 Variant Implicated in Autosomal Dominant Retinitis
895   Pigmentosa. *Hum Gene Ther*. 2023;34(13-14):639-648.
896   doi:10.1089/hum.2022.240

897 70. Birtel J, von Landenberg C, Gliem M, et al. Mitochondrial Retinopathy. *Ophthalmol*
898   *Retina*. 2022;6(1):65-79. doi:10.1016/j.oret.2021.02.017

899 71. Marlhens F, Bareil C, Griffoin JM, et al. Mutations in RPE65 cause Leber's
900   congenital amaurosis. *Nat Genet*. 1997;17(2):139-141. doi:10.1038/ng1097-139

901 72. Gu S min, Thompson DA, Srikumari CRS, et al. Mutations in RPE65 cause
902   autosomal recessive childhood–onset severe retinal dystrophy. *Nat Genet*.
903   1997;17(2):194-197. doi:10.1038/ng1097-194

904 73. Kenna PF, Humphries MM, Kiang AS, et al. Advanced late-onset retinitis
905   pigmentosa with dominant-acting D477G RPE65 mutation is responsive to oral
906   synthetic retinoid therapy. *BMJ Open Ophth*. 2020;5:462. doi:10.1136/bmjophth-
907   2020-000462

908 74. Mendes HF, Van Der Spuy J, Chapple JP, Cheetham ME. Mechanisms of cell death
909   in rhodopsin retinitis pigmentosa: Implications for therapy. *Trends Mol Med*.
910   2005;11(4):177-185. doi:10.1016/j.molmed.2005.02.007

911   75.   Wilson John H. WTG. The Nature of Dominant Mutations of Rhodopsin and
912   Implications for Gene Therapy. *Mol Neurobiol*. 2003;28.
913   76.   Murray SF, Jazayeri A, Matthes MT, et al. Allele-specific inhibition of rhodopsin
914   with an antisense oligonucleotide slows photoreceptor cell degeneration. *Invest*
915   *Ophthalmol Vis Sci*. 2015;56(11):6362-6375. doi:10.1167/iovs.15-16400
916   77.   She K, Liu Y, Zhao Q, et al. Dual-AAV split prime editor corrects the mutation and
917   phenotype in mice with inherited retinal degeneration. *Signal Transduct Target*
918   *Ther*. 2023;8(1). doi:10.1038/s41392-022-01234-1
919   78.   Qin H, Zhang W, Zhang S, et al. Vision rescue via unconstrained in vivo prime
920   editing in degenerating neural retinas. *Journal of Experimental Medicine*.
921   2023;220(5). doi:10.1084/jem.20220776
922   79.   Maeder ML, Stefanidakis M, Wilson CJ, et al. Development of a gene-editing
923   approach to restore vision loss in Leber congenital amaurosis type 10. *Nat Med*.
924   2019;25(2):229-233. doi:10.1038/s41591-018-0327-9
925   80.   Pierce EA, Aleman TS, Jayasundera KT, et al. Gene Editing for CEP290 -Associated
926   Retinal Degeneration . *New England Journal of Medicine*. 2024;390(21):1972-
927   1984. doi:10.1056/nejmoa2309915
928
929

Tables

Table 1. Demographics, phenotype, genetic testing method used to identify the c.1555G>A p.(E519K) RPE65 variant and optional remarks for each
patient.

ID	Sex	Age at last exam (y)	Age at onset/diagnosis (y)	Phenotype	Genetic testing	Remarks
F1-I:1	M	61	61	Pattern Dystrophy	Targeted sequencing (segregation)	
F1-II:1	F	29	18	Mottled Phenotype	WES RetNet	
F2-I:1	M	90	90	Pattern Dystrophy	Targeted sequencing (segregation)	Left eye excluded due to trauma; right eye BCVA excluded due to cognitive problems
F2-II:1	F	63	63	Mottled Phenotype	Targeted sequencing (segregation)	
F2-III:1	F	34	18	Mottled Phenotype	WES RetNet	
F3-II:2	F	75	72	Pattern Dystrophy	WES RetNet	
F3-II:4	M	72	72	Pattern Dystrophy	Targeted sequencing (segregation)	
F3-III:4	F	48	47	Mottled Phenotype	Targeted sequencing (segregation)	
F3-III:6	F	45	45	Mottled Phenotype	Targeted sequencing (segregation)	
F3-III:8	F	38	38	Mottled Phenotype	Targeted sequencing (segregation)	
F4-I:1	M	79	72	Pattern Dystrophy	WES RetNet	
F4-II:1	M	58	58	Pattern Dystrophy	Targeted sequencing (segregation)	
F4-III:1	F	18	18	Mottled Phenotype	Targeted sequencing (segregation)	
F5-III:1	F	75	74	Pattern Dystrophy	Targeted sequencing (segregation)	
F5-III:2	M	69	60	Pattern Dystrophy	WGS RetNet	

F5-III:4	F	70	65	Pattern Dystrophy	Targeted sequencing (segregation)	
F5-III:5	F	68	64	Pattern Dystrophy	Targeted sequencing (segregation)	
F5-III:6	F	67	63	Mottled Phenotype	Targeted sequencing (segregation)	
F5-III:7	F	62	58	Pattern Dystrophy	Targeted sequencing (segregation)	
F5-III:8	F	60	56	Mottled Phenotype	Targeted sequencing (segregation)	
F5-IV:3	F	41	41	Pattern Dystrophy	WGS RetNet	
F6-I:1	M	68	33	Mottled Phenotype	Targeted sequencing (segregation)	
F6-II:1	F	41	29	Mottled Phenotype	WES RetNet	
F7-I:1	M	65	62	Mottled Phenotype	Targeted sequencing (segregation)	
F7-II:1	F	40	36	Mottled Phenotype	WES RetNet	
F8-II:3	M	65	58	Pattern Dystrophy	Targeted sequencing (segregation)	
F8-II:5	M	62	45	Pattern Dystrophy	WGS RetNet	
F8-III:1	F	40	40	Mottled Phenotype	Targeted sequencing (segregation)	
F8-III:2	F	37	37	Mottled Phenotype	Targeted sequencing (segregation)	
F9-I:1	M	72	72	Pattern Dystrophy	Targeted sequencing (segregation)	
F9-II:1	M	42	37	Mottled Phenotype	WES RetNet	
F10-II:1	M	68	NA	Autosomal recessive RCD	WES RetNet	IRD due to *ZNF408*: c.[16G>T];[16G>T], p.[(Glu6Ter)];[(Glu6Ter)]
F10-III:2	F	35	31	Mottled Phenotype	Targeted sequencing (segregation)	
F11-II:1	F	53	48	Mottled Phenotype	WES RetNet	Compound heterozygous carrier of two *ABCC6* variants without PXE phenotype
F11-II:2	F	46	39	Mottled Phenotype	Targeted sequencing (segregation)	BCVA excluded due to history of bilateral optic neuritis
F12-I:1	F	70	70	Mottled Phenotype	Targeted sequencing (segregation)	

F12-II:1	F	31	31	Mottled Phenotype	Targeted sequencing (specific phenotype)	
F13-I:1	M	86	70	Pattern Dystrophy	Targeted sequencing (segregation)	
F13-II:2	M	59	31	Pattern Dystrophy	Targeted sequencing (*PRPH2* negative cohort)	
F13-II:4	F	55	48	Pattern Dystrophy	Targeted sequencing (segregation)	
F13-III:1	F	30	30	Mottled Phenotype	Targeted sequencing (segregation)	
F13-III:3	F	27	27	Mottled Phenotype	Targeted sequencing (segregation)	
F14-I:1	M	81	75	Pattern Dystrophy	WES RetNet	
F14-II:1	M	57	57	Pattern Dystrophy	Targeted sequencing (segregation)	
S01	M	44	24	Mottled Phenotype	WES RetNet	
S02	M	44	35	Mottled Phenotype	WES RetNet	
S03	F	49	49	Mottled Phenotype	WES RetNet	
S04	F	51	50	Pattern Dystrophy	WES RetNet	
S05	M	54	49	Pattern Dystrophy	WES RetNet	
S06	M	57	55	Pattern Dystrophy	WES RetNet	
S07	M	57	57	Pattern Dystrophy	WES RetNet	
S08	F	59	59	Pattern Dystrophy	Targeted sequencing (*ABCA4* negative cohort)	
S09	F	59	54	Pattern Dystrophy	Targeted sequencing (MIDD negative cohort)	
S10	F	59	56	Pattern Dystrophy	WES RetNet	

S11	M	64	57	Pattern Dystrophy	Targeted sequencing (MIDD negative cohort)	
S12	F	66	59	Pattern Dystrophy	WES RetNet	
S13	M	67	57	Mottled Phenotype	Targeted sequencing (MIDD negative cohort)	BCVA excluded due to idiopathic congenital nystagmus
S14	M	70	70	Pattern Dystrophy	Targeted sequencing (MIDD negative cohort)	
S15	M	73	70	NA	WES RetNet	Short-wavelength autofluorescence imaging not performed
S16	M	77	76	Pattern Dystrophy	WES RetNet	Hemizygous carrier of *CACNA1F* variant without CSNB phenotype (normal ffERG)
S17	M	77	72	Pattern Dystrophy	Targeted sequencing (MIDD negative cohort)	
S18	M	78	74	Pattern Dystrophy	Targeted sequencing (MIDD negative cohort)	
S19	F	81	75	Pattern Dystrophy	WES RetNet	
S20	F	78	NA	Leber Congenital Amaurosis	WES RetNet	IRD due to *CEP290*: c.[4723A>T];[2991+1655A>G], p.[(Lys1575Ter)];[?]
S21	F	72	71	Pattern Dystrophy	Targeted sequencing (*PRPH2* negative cohort)	
S22	F	55	55	RCD/RP	WES RetNet	External patient (Belgium) Toxic alcohol/tobacco-related optic neuropathy
S23	M	65	58	Mottled Phenotype	WES RetNet	External patient (Belgium)

F15-I:1	M	82	55	Pattern Dystrophy	Targeted sequencing (segregation)	External patient (Belgium)
F15-II:1	F	60	57	Pattern Dystrophy	WES RetNet	External patient (Belgium)
S24	M	58	48	Pattern Dystrophy	WES RetNet	External patient (Belgium)
S25	M	44	39	Mottled Phenotype	Targeted sequencing (*PRPH2* & *BEST1* negative cohort)	External patient (Belgium)
S26	F	65	65	Pattern Dystrophy	Targeted sequencing (*PRPH2* & *BEST1* negative cohort)	External patient (Belgium)
S27	M	70	63	Pattern Dystrophy	Targeted sequencing (MIDD negative cohort)	External patient (Belgium)
S28	M	69	55	Pattern Dystrophy	Targeted sequencing (MIDD negative cohort)	External patient (Belgium)
S29	M	40	37	Pattern Dystrophy	WES RetNet	External patient (Belgium)
F16-II:1	F	44	33	Mottled Phenotype	Retinal Dystrophy Panel (Blueprint Genetics)	External patient (Canada)
F16-II:2	F	40	35	Mottled Phenotype	Retinal Dystrophy Panel (Blueprint Genetics)	External patient (Canada)
S30	M	57	55	Mottled Phenotype	Inherited Retinal Disorders Panel (Invitae)	External patient (Canada)
S31	F	38	35	Mottled Phenotype	Inherited Retinal Disorders Panel (Invitae)	External patient (Canada)
S32	M	72	60-70	Pattern Dystrophy	Retinal Dystrophy Panel (Blueprint Genetics)	External patient (Canada)

S33	M	65	50-60	Pattern Dystrophy	Retinal Dystrophy Panel (Blueprint Genetics)	External patient (Canada)
S34	M	24	17	Mottled Phenotype	Targeted sequencing 226 IRD genes	External patient (France)
S35	M	73	NA	Pattern Dystrophy	WES Vision disorders (505 IRD genes)	External patient (Netherlands)

External patients were seen in Belgian clinical centers other than Department of Ophthalmology at Ghent University Hospital. Abbreviations used: M = male; F = female; RCD = rod cone dystrophy; WES = whole exome sequencing; WGS = whole genome sequencing; MIDD = Maternally Inherited Diabetes and Deafness; NA = not available/applicable; PXE = Pseudoxanthoma elasticum ; CSNB = Congenital Stationary Night Blindness ; ERG = Electroretinogram.

935

Supplementary Files

This is a list of supplementary files associated with this preprint. Click to download.

- Supplementalfiguresandtables.pdf